Atmos. Chem. Phys., 22, 8951–8971, 2022
https://doi.org/10.5194/acp-22-8951-2022

Atmospheric Chemistry and Physics
Open Access
EGU

Budget of nitrous acid (HONO) at an urban site in the fall season of Guangzhou, China

Yihang Yu[1,2], Peng Cheng[1,2,5], Huirong Li[1,2], Wenda Yang[1,2], Baobin Han[1,2], Wei Song[3], Weiwei Hu[3], Xinming Wang[3], Bin Yuan[4,5], Min Shao[4,5], Zhijiong Huang[4], Zhen Li[4], Junyu Zheng[4,5], Haichao Wang[6], and Xiaofang Yu[1,2]

[1]Institute of Mass Spectrometry and Atmospheric Environment, Jinan University, Guangzhou 510632, China
[2]Guangdong Provincial Engineering Research Center for Online Source Apportionment System of Air Pollution, Guangzhou 510632, China
[3]State Key Laboratory of Organic Geochemistry, Guangzhou Institute of Geochemistry, Chinese Academy of Sciences, Guangzhou 510640, China
[4]Institute for Environmental and Climate Research, Jinan University, Guangzhou 511443, China
[5]Guangdong–Hong Kong–Macau Joint Laboratory of Collaborative Innovation for Environmental Quality, Guangzhou 511443, China
[6]School of Atmospheric Sciences, Sun Yat-Sen University, Zhuhai, China

Correspondence: Peng Cheng (chengp@jnu.edu.cn)

Received: 5 March 2021 – Discussion started: 3 May 2021
Revised: 9 June 2022 – Accepted: 10 June 2022 – Published: 12 July 2022

Abstract. High concentrations of nitrous acid (HONO) have been observed in the Pearl River Delta (PRD) region of China in recent years, contributing to an elevated atmospheric oxidation capacity due to the production of OH through HONO photolysis. We investigated the budget of HONO at an urban site in Guangzhou from 27 September to 9 November 2018 using data from a comprehensive atmospheric observation campaign. During this period, measured concentrations of HONO were 0.02 to 4.43 ppbv, with an average of 0.74 ± 0.70 ppbv. An emission ratio ($HONO/NO_x$) of 0.9 ± 0.4 % was derived from 11 fresh plumes. The primary emission rate of HONO at night was calculated to be between 0.04 ± 0.02 and 0.30 ± 0.15 ppbv h^{-1} based on a high-resolution NO_x emission inventory. Heterogeneous conversion of NO_2 on the ground surface (0.27 ± 0.13 ppbv h^{-1}), primary emissions from vehicle exhaust (between 0.04 ± 0.02 and 0.30 ± 0.15 ppbv h^{-1}, with a middle value of 0.16 ± 0.07 ppbv h^{-1}), and the homogeneous reaction of NO + OH (0.14 ± 0.30 ppbv h^{-1}) were found to be the three largest sources of HONO at night. Heterogeneous NO_2 conversion on aerosol surfaces (0.03 ± 0.02 ppbv h^{-1}) and soil emission (0.019 ± 0.009 ppbv h^{-1}) were two other minor sources. Correlation analysis shows that NH_3 and the relative humidity (RH) may have participated in the heterogeneous transformation of NO_2 to HONO at night. Dry deposition (0.41 ± 0.31 ppbv h^{-1}) was the main removal process of HONO at night, followed by dilution (0.18 ± 0.16 ppbv h^{-1}), while HONO loss at aerosol surfaces was much slower (0.008 ± 0.006 ppbv h^{-1}). In the daytime, the average primary emission P_{emis} was 0.12 ± 0.02 ppbv h^{-1}, and the homogeneous reaction P_{OH+NO} was 0.79 ± 0.61 ppbv h^{-1}, larger than the unknown source $P_{Unknown}$ (0.65 ± 0.46 ppbv h^{-1}). Similar to previous studies, $P_{Unknown}$ appeared to be related to the photo-enhanced conversion of NO_2.

Our results show that primary emissions and the reaction of NO + OH can significantly affect HONO at a site with intensive emissions during both the daytime and nighttime. Uncertainty in parameter values assumed in the calculation of HONO sources can have a strong impact on the relative importance of HONO sources at night, and could be reduced by improving knowledge of key parameters such as the NO_2 uptake coefficient. The uncertainty in the estimated direct emission can be reduced by using emission data with higher resolution and quality. Our study highlights the importance of better constraining both conventional and novel HONO sources by reducing uncertainties in their key parameters for advancing our knowledge of this important source of atmospheric OH.

Published by Copernicus Publications on behalf of the European Geosciences Union.

1 Introduction

Nitrous acid (HONO) is an important primary source of hydroxyl radical (OH) through photolysis (Reaction R1), contributing up to 33 %–92 % of the OH at rural and urban sites (Kleffmann et al., 2005; Michoud et al., 2012; Tan et al., 2017; Xue et al., 2020; Hendrick et al., 2014).

$$\mathrm{HONO} + h\nu \rightarrow \mathrm{OH} + \mathrm{NO}\,(300\,\mathrm{nm} < \lambda < 405\,\mathrm{nm}) \quad \text{(R1)}$$

OH is the principal atmospheric oxidant responsible for oxidizing and removing most natural and anthropogenic trace gases. OH initiates the oxidation of volatile organic compounds (VOC) to produce hydroperoxyl radicals (HO_2) and organic peroxy radicals (RO_2), which further leads to the formation of ground-level ozone (O_3) in the presence of nitrogen oxides ($NO_x = NO + NO_2$) (Xue et al., 2016; Finlayson-Pitts and Pitts, 2000; Hofzumahaus et al., 2009; Lelieveld et al., 2016; Tan et al., 2018) as well as secondary organic aerosols (SOA). However, the detailed formation mechanisms of HONO are still not well understood, and the observed HONO concentrations cannot be completely explained by current knowledge (Sörgel et al., 2011a; Kleffmann et al., 2005; Liu et al., 2019a; Lee et al., 2016; Liu et al., 2020b; Pusede et al., 2015). So far, numerous HONO sources have been found, and they can be categorized as direct emissions, homogeneous reactions, and heterogeneous reactions. Fossil fuel combustion is the most important direct emission source of HONO (Kurtenbach et al., 2001; Kirchstetter et al., 1996; Rappenglück et al., 2013; Kramer et al., 2020; Xu et al., 2015; Trinh et al., 2017). In general, the emission ratios $HONO/NO_x$ obtained from fresh air masses mixed with vehicle exhaust (0.03 %–1.7 %) (Kurtenbach et al., 2001; Kirchstetter et al., 1996; Rappenglück et al., 2013; Trinh et al., 2017; Liu et al., 2017; Pitts et al., 1984; Nakashima and Kajii, 2017) are much smaller than the ratios $HONO/NO_x$ observed in the low boundary layer (2.3 %–9 %) (Yang et al., 2014; Zhou et al., 2002a; Hao et al., 2020; Gu et al., 2021; Li et al., 2018a; Yu et al., 2009; Acker et al., 2006; Kleffmann et al., 2003; VandenBoer et al., 2013; Vogel et al., 2003), reflecting substantial secondary formation of HONO away from direct emissions. Recent studies have found that soil might be another major source of direct HONO emissions (Su et al., 2011; Oswald et al., 2013; Weber et al., 2015; Wu et al., 2019; Y. Wang et al., 2021), although the confirmation of its atmospheric significance requires further comparisons between laboratory and field measurements. It should be noted that direct emissions may surpass secondary sources at sampling sites with heavy emission impacts (Liu et al., 2019a; Tong et al., 2015; Zhang et al., 2019; Tong et al., 2016; Meusel et al., 2016).

The homogeneous gas-phase reaction between NO and OH (Reaction R2) is the most well-known secondary source of HONO (Perner and Platt, 1979). HONO concentrations measured in the atmosphere cannot be explained by direct emissions and this reaction alone, especially during the daytime (Kleffmann et al., 2005; Lee et al., 2016), when a large source of HONO is necessary to sustain the measured level of HONO against fast photolysis. Some homogeneous HONO formation mechanisms have been proposed to explain the gap between the observed and predicted HONO, including HONO formation by photolysis of *o*-nitrophenol (Bejan et al., 2006; W. Yang et al., 2021) and the reaction of NO_2 with $HO_2{\cdot}H_2O$ (X. Li et al., 2014). However, they are yet to be confirmed to occur in the atmosphere, and are unlikely to be the main HONO source.

$$\mathrm{NO} + \mathrm{OH} \rightarrow \mathrm{HONO} \quad \text{(R2)}$$

$$2\mathrm{NO_2} + \mathrm{H_2O} \rightarrow \mathrm{HONO} + \mathrm{HNO_3\,(surface)} \quad \text{(R3)}$$

$$\mathrm{NO_2} + \mathrm{red_{ads}} \rightarrow \mathrm{HONO} + \mathrm{ox_{ads}} \quad \text{(R4)}$$

Heterogeneous reactions of NO_2 on various surfaces have drawn substantial interest due to the observed correlation between HONO and NO_2 during many field observations. Vertical gradient observations suggest that HONO is more likely produced from the ground surface (Wong et al., 2012; Kleffmann et al., 2003; Stutz et al., 2002; VandenBoer et al., 2013; Wong et al., 2011; Villena et al., 2011), while some observations have found a good correlation between HONO and aerosol surface area (Reisinger, 2000; Su et al., 2008a; Jia et al., 2020; Zheng et al., 2020; Liu et al., 2014), which can be related to the concentration and composition of particulate matter (Cui et al., 2018; Liu et al., 2014; Colussi et al., 2013; Yabushita et al., 2009; Kinugawa et al., 2011). Both laboratory studies and field observations have found that hydrolysis of NO_2 on wet surfaces can produce HONO (Reaction R3), and the uptake coefficient of NO_2 (γ) can vary by several orders of magnitude (Finlayson-Pitts et al., 2003; Stutz et al., 2004; Acker et al., 2004). HONO can also be generated by NO_2 reduction on various surfaces (soot, semivolatile organic compounds, humic acid, etc.) (Reaction R4) at a much faster rate than NO_2 hydrolysis, but the surfaces could be inactivated in a short period of time (Ammann et al., 1998; Han et al., 2017a, 2017b; Gerecke et al., 1998; Monge et al., 2010; Gutzwiller et al., 2002; Wall and Harris, 2017; Stemmler et al., 2006; Aubin and Abbatt, 2007). However, irradiation could enhance the reaction and maintain the activity of the surfaces, making it possible for it to play an important role in HONO formation during daytime. Both laboratory and field studies found that photolysis of adsorbed HNO_3 and particulate nitrate (NO_3^-) could produce HONO (Ye et al., 2016, 2017; Zhou et al., 2003, 2002b, 2011), which might be an important HONO source, at least in remote areas and polar regions. Evidence of other new pathways and mechanisms has also been found and their atmospheric relevance discussed (Ge et al., 2019; Wang et al., 2016; Xu et al., 2019; L. Li et al., 2018; Xia et al., 2021; Zhao et al., 2021; Gen et al., 2021).

The Pearl River Delta (PRD) region is one of the biggest city clusters in the world, with a dense population and large anthropogenic emissions. Rapid economic development and urbanization have led to severe air pollution in this region, which has been characterized by atmospheric "compound pollution" with concurrently high fine particulate matter ($PM_{2.5}$) and ozone (O_3) (Tang, 2004; Chan and Yao, 2008; Yue et al., 2010; T. Wang et al., 2017; Xue et al., 2014; Zheng et al., 2010). In recent years, O_3 has been increasing along with reduced $PM_{2.5}$ in the region (J. Li et al., 2014; Liao et al., 2020; Wang et al., 2009; Zhong et al., 2013; Lu et al., 2018), and this has become the dominant reason that the air quality index exceeds the national standard (Feng et al., 2019), indicating an enhancement of the atmospheric oxidation capacity. So far, two comprehensive atmospheric observations have been conducted in the PRD region, focusing on the balance and dynamics of OH sources and sinks (Hofzumahaus et al., 2009; Tan et al., 2019). A substantial amount of HONO was suggested to be a major source of the OH–HO_2–RO_2 radical system in these two campaigns (Lu et al., 2012; Tan et al., 2019) as well as in other previous campaigns (Hu et al., 2002; Su et al., 2008a, b; Qin et al., 2009; Li et al., 2012; Shao et al., 2004).

In this work, we performed continuous measurements of HONO, along with trace gases, photolysis frequencies, and meteorological conditions, at an urban site in Guangzhou from 27 September to 9 November 2018 as part of the field campaign "Particles, Radicals, Intermediates from oxiDation of primary Emissions in Greater Bay Area" (PRIDE-GBA2018). Benefiting from numerous prior field observational studies in the PRD region, our study is strongly positioned to ensure high-quality data acquisition and analysis of HONO along with a full suite of other chemical species, providing a unique and valuable opportunity to refine our knowledge of HONO sources and sinks as well as the role of HONO in the photochemistry of O_3 and OH in such a region with extensive air pollution as well as rigorous emission control in recent years.

Departing from the valuable knowledge and experiences gained from numerous previous HONO studies in the PRD region and around the world, we aim to draw useful and unique insights from a detailed analysis of our dataset in the context of a comprehensive review of previous data and findings, with special attention paid to reducing and/or characterizing the uncertainties in parameterizations and their implications for the relative importance of various HONO sources and sinks. Specifically, (1) a high-resolution (3 km × 3 km) NO_x emission inventory for Guangzhou City (Huang et al., 2021) was used to estimate the primary emission rates of NO_x and HONO, which would reduce the uncertainty of the HONO primary emission rate; (2) a wide range of possible parameter values have been evaluated for each source to quantify their strengths and rank their importance; and (3) uncertainties associated with each source and other possible factors are discussed in detail.

2 Experiment

2.1 Observation site

The sampling site (23.14° N, 113.36° E) is located in the Guangzhou Institute of Geochemistry Chinese Academy of Sciences (GIGCAS). The instruments were deployed in the cabin on the rooftop of a seven-story building (∼ 40 m above the ground). The site is surrounded by residential communities and schools with no industrial manufacturers or power plants around, thus representing a typical urban environment in the PRD region. The South China Expressway and Guangyuan Expressway, both with heavy traffic loading, are located west and south of the site at distances of about 300 m. As a result, the site often experienced local emissions from traffic. The location and surroundings of the site are shown in Fig. S1 in the Supplement.

2.2 Measurements

HONO was measured by a custom-built LOPAP (long-path absorption photometer) (Heland et al., 2001; Kleffmann et al., 2006). More information about our custom-built LOPAP (including its principle, quality assurance/quality control, instrument parameters, and an intercomparison) are introduced in the Supplement.

In addition to HONO, NO_x ($NO + NO_2$) was measured by a nitrogen oxide analyzer (Thermo Scientific, model 42i), which used a NO-NO_x chemiluminescence detector equipped with a molybdenum-based converter with a time resolution and detection limit of 1 min and 0.4 ppbv, respectively. It should be noted that molybdenum oxide (MoO) converters may also convert some NO_z ($= NO_y - NO_x$) (e.g., HONO, peroxyacetyl nitrate (PAN), HNO_3, and so on) species to NO and hence could overestimate the ambient NO_2 concentrations. The degree of overestimation depends on both the air mass age and the composition of NO_y. At our site, which was greatly affected by fresh emissions, the relative interferences of NO_z with NO_2 have been estimated to be around 10 % (see the Supplement), which is close to the results of Xu et al. (2013) and negligible for our discussion of the HONO budget. O_3 was measured by an O_3 analyzer (Thermo Scientific, model 49i) via an ultraviolet absorption method with a time resolution and detection limit of 1 min and 1 ppbv, respectively. SO_2 was measured by an SO_2 analyzer (Thermo Scientific, model 43i) via a pulsed fluorescence method with a time resolution and detection limit of 1 min and 0.5 ppbv, respectively. CO was measured by a CO analyzer (Thermo Scientific, model 48i) with a time resolution and detection limit of 1 min and 0.04 ppmv, respectively. NH_3 was measured by laser absorption spectroscopy (PICARRO, G2508) with a precision of <3 ppbv at 1 min. Gaseous HNO_3 was detected by a time-of-flight chemical ionization mass spectrometer (Aerodyne Research Inc., TOF-CIMS) with a time resolution of 1 min.

Particulate nitrate (NO_3^-) was measured by a time-of-flight aerosol mass spectrometer (Aerodyne Research Inc., TOF-AMS) with a time resolution of 1 min. $PM_{2.5}$ was measured by a beta attenuation monitor (MET One Instruments Inc., BAM-1020) with a time resolution and detection limit of 1 h and 4.0 $\mu g\,m^{-3}$, respectively. The meteorological data, including temperature (T), relative humidity (RH), and wind speed and direction (WS, WD), were recorded by a Vantage Pro2 weather station (Davis Instruments Inc.) with a time resolution of 1 min. Photolysis frequencies, including $J(HONO)$, $J(NO_2)$, and $J(O^1D)$, were measured by a spectrometer (Focused Photonics Inc., PFS-100) with a time resolution of 1 min.

3 Results and discussion

3.1 Data overview

The time series of meteorological parameters and pollutants during the campaign are shown in Fig. 1. The HONO concentrations ranged from 0.02 to 4.43 ppbv, with an average of 0.74 ± 0.70 ppbv. Table 1 summarizes the HONO observations reported in the PRD region since 2002. HONO appears to have shown a decreasing trend in Guangzhou, as an improvement in air quality in Guangzhou was witnessed during the past decade. Spikes of NO occurred frequently, even up to 134.8 ppbv, as a result of traffic emissions from two major roads near the site. The concentrations of NO_2, SO_2, NH_3, and $PM_{2.5}$ were 5.4–102.0, 0–6.3, 2.8–7.8 ppbv, and 4–109 $\mu g\,m^{-3}$, respectively, with average values of 50.8 ± 17.2, 1.9 ± 1.2, 6.3 ± 2.7 ppbv, and $36 \pm 16\,\mu g\,m^{-3}$, respectively. The O_3 concentration ranged from 0.3 to 149.8 ppbv with an average peak concentration of 73.9 ± 28.4 ppbv. During the observations, the temperature ranged from 17 to 30 °C with an average of 24 ± 3 °C, and the relative humidity ranged from 28 % to 97 % with an average of 70 ± 17 %. The average wind speed was $6.8 \pm 4.5\,m\,s^{-1}$, while the maximum wind speed was $22.7\,m\,s^{-1}$. There was a pollution period from 8 to 10 October with elevated $PM_{2.5}$ ($60 \pm 12\,\mu g\,m^{-3}$) and HONO (0.94 ± 0.58 ppbv). By contrast, from 29 October to 3 November, efficient ventilation driven by strong winds ($>11\,m\,s^{-1}$) led to low levels of most pollutants in this period, with average concentrations of $PM_{2.5}$ and HONO at $28 \pm 11\,\mu g\,m^{-3}$ and 0.56 ± 0.34 ppbv, respectively.

The time series of the photolysis frequencies $J(HONO)$, $J(O^1D)$, and $J(NO_2)$ across the whole observation period are shown in Fig. S3. The maximum values of $J(HONO)$, $J(O^1D)$ and $J(NO_2)$ are 1.58×10^{-3}, 2.54×10^{-5}, and $9.31 \times 10^{-3}\,s^{-1}$, respectively. These J values tracked a similar diurnal pattern, reaching a maximum at noon (with high solar radiation) and decreasing to zero at night.

The diurnal variations of HONO, NO_2, $HONO/NO_2$, and NO are shown in Fig. 2. A daytime trough and a nighttime peak of HONO were observed, as typically seen at urban and rural sites (Lee et al., 2016; Xue et al., 2020; Villena et al., 2011; Y. Yang et al., 2021). The observed high HONO concentration of around 0.5 ppbv in the daytime implies strong HONO production to balance its rapid loss through photolysis. NO_2 showed a similar diurnal pattern. It is worth noting that the diurnal variation of NO was quite similar to that of HONO, implying a potential association between them. Additionally, the observed large amount of NO (10.8 ± 17.2 ppbv) at night indicated strong primary emission near the site. The ratio $HONO/NO_2$, an indicator of NO_2 to HONO conversion, rose at night and decreased after sunrise due to photolysis, ranging from 0.002 to 0.091 with an average of 0.023 ± 0.013, which is lower than most previous field observations in the PRD region (Li et al., 2012; Qin et al., 2009; Xu et al., 2015) and is typical of relatively fresh plumes (Febo et al., 1996; Lammel and Cape, 1996; Sörgel et al., 2011b; Stutz et al., 2004; Zhou et al., 2007; Su et al., 2008a).

3.2 Nocturnal HONO sources and sinks

3.2.1 Direct emissions

As noted in Sect. 2.1, the site was expected to receive substantial direct emissions of HONO from two major roads nearby. We obtained the emitted $HONO/NO_x$ ratios in fresh plumes defined with the following criteria (Xu et al., 2015): (a) $NO_x > 49.7$ ppbv (highest 25 % of the NO_x data); (b) $NO/NO_x > 0.8$; (c) good correlation between NO_x and HONO ($R^2 > 0.70$, $P < 0.05$); (d) short plume duration (<2 h); and (e) global radiation $< 10\,W\,m^{-2}$ ($J(NO_2) < 0.25 \times 10^{-3}\,s^{-1}$).

During the campaign, 11 fresh plumes were found to satisfy all of the criteria (see Table S2 in the Supplement). Two cases among them are shown in Fig. S4. The $HONO/NO_x$ ratios in these selected plumes varied from 0.1 % to 1.5 % with an average value of 0.9 ± 0.4 %, which is comparable to the average values of 1.2 % (Xu et al., 2015) and 1.0 % (Yun et al., 2017) measured in Hong Kong, 0.79 % measured in Nanjing (Liu et al., 2019b), and 0.69 % observed in Changzhou (Shi et al., 2020). It should be noted that the emission factor derived in this study was based on field observation and the screening criterion for fresh air mass was $NO/NO_x > 0.8$, while the fresh air mass was characterized by $NO/NO_x > 0.9$ in the tunnel experiments conducted by Kurtenbach et al. (2001), so the air masses we selected were still slightly aged and the emission factor derived in this study is slightly overestimated.

To quantify the primary emission rate of HONO, three methods have been used in previous studies (Liu et al., 2019b; Liu et al., 2020a; Meng et al., 2020). In method (1), the observed NO_x concentration is assumed to represent the accumulation of emissions, but the sinks of NO_x and HONO are ignored, as are transport and convection. On this basis, $[HONO]_{emis}$ (the primary emission contribution to the HONO concentration) is estimated as the product of

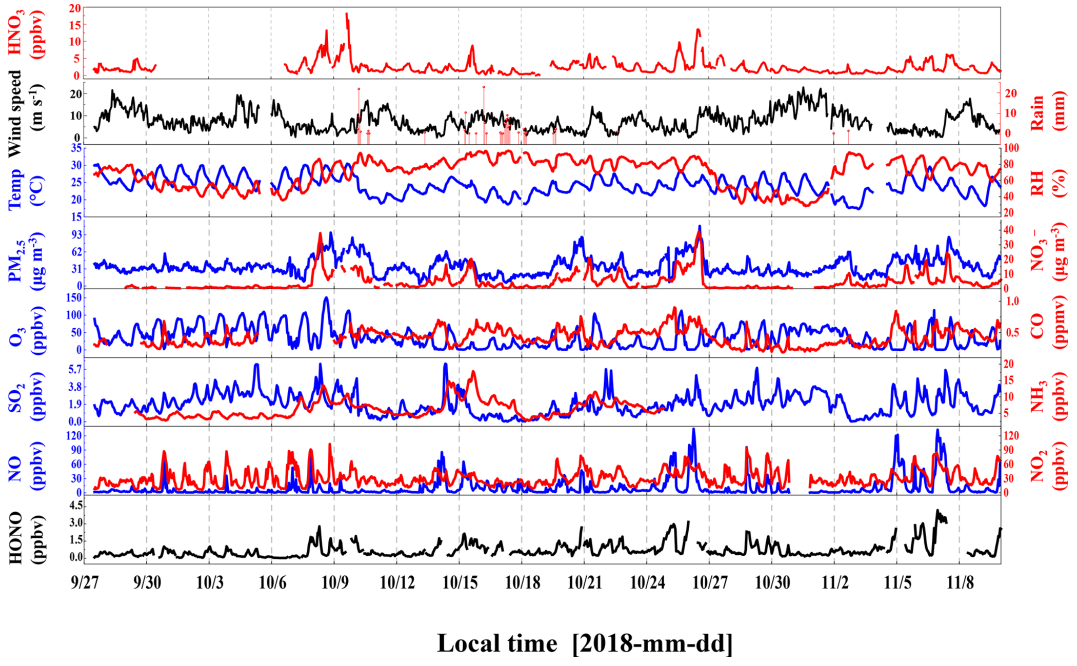

Figure 1. Temporal variations of meteorological parameters and pollutants during the observation period.

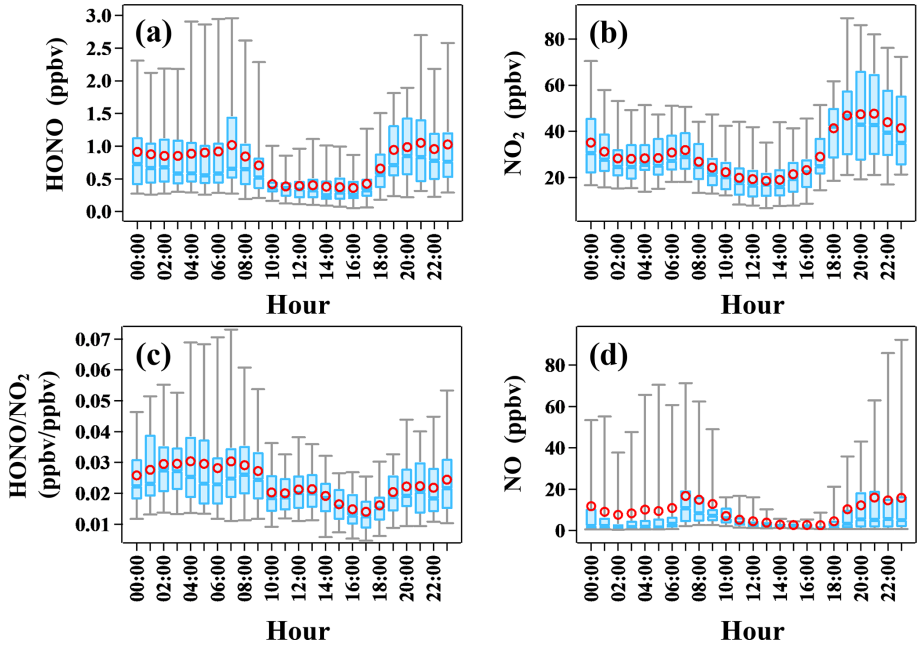

Figure 2. Diurnal profiles of **(a)** HONO, **(b)** NO_2, **(c)** HONO/NO_2, and **(d)** NO during the observation period. In each box, the blue line and the red circle refer to the median and mean, respectively. The upper and lower boundaries of each box represent the 75th and the 25th percentiles; the whiskers above and below each box represent the 95th and 5th percentiles. The box plots presented in this study were generated by an Igor-Pro-based computer program, Histbox (Wu et al., 2018).

Table 1. Overview of the ambient HONO, NO_2, and NO_x measurements as well as the HONO/NO_2 ratios in the PRD region ordered chronologically. Data from Guangzhou are in italics.

Location	Date	HONO (ppbv)	HONO (ppbv)		NO_2 (ppbv)		NO_x (ppbv)		HONO/NO_2		Reference
			Night	Day	Night	Day	Night	Day	Night	Day	
Guangzhou (China)	*July 2002*	*1.89*	–	–	–	–	–	–	–	–	*1*
	November 2002	*1.52*	–	–	–	–	–	–	–	–	
Xinken (China)	*October–November 2004*	*1.20*	*1.30*	*0.80*	*34.8*	*30.0*	*37.8*	*40.0*	*0.037*	*0.027*	*2*
Back Garden (China)	*July 2006*	*0.93*	*0.95*	*0.24*	*16.5*	*4.5*	*20.9*	*5.5*	*0.057*	*0.053*	*3*
Guangzhou (China)	*July 2006*	*2.80*	*3.50*	*2.00*	*20.0*	*30.0*	–	–	*0.175*	*0.067*	*4*
Guangzhou (China)	*October 2015*	*1.64*	*2.25*	*0.90*	*40.5*	*27.3*	*57.9*	*39.8*	*0.060*	*0.030*	*5*
Guangzhou (China)	*July 2016*	*1.03*	*1.27*	*0.70*	*35.0*	*25.9*	*66.3*	*52.1*	*0.040*	*0.070*	*6*
Guangzhou (China)	*September–November 2018*	*0.74*	*0.91*	*0.44*	*36.9*	*23.3*	*47.7*	*30.1*	*0.026*	*0.022*	–
Jiangmen (China)	October–November 2008	0.60	–	0.48	–	–	–	9.1	–	–	7
Hong Kong (China)	August 2011	0.66	0.66	0.70	21.8	18.1	29.3	29.3	0.031	0.042	8
	November 2011	0.93	0.95	0.89	27.2	29.0	37.2	40.6	0.034	0.030	
	February 2012	0.91	0.88	0.92	22.2	25.8	37.8	48.3	0.036	0.035	
	May 2012	0.35	0.33	0.40	14.7	15.0	19.1	21.1	0.022	0.030	
Hong Kong (China)	September–December 2012	0.13	–	–	–	–	–	–	–	–	9
Heshan (China)	October 2013	1.57	–	–	–	–	–	–	–	–	10
Heshan (China)	October–November 2014	1.40	1.78	0.77	19.3	17.9	21.5	22.7	0.093	0.055	11
Hong Kong (China)	March–May 2015	3.30	2.86	3.91	–	–	–	–	–	–	12
Heshan (China)	January 2017	2.70	3.10	2.30	–	–	–	–	0.116	0.089	13

References: 1: Hu et al. (2002); 2: Su et al. (2008a) and (2008b); 3: Su (2008) and Li et al. (2012); 4: Qin et al. (2009); 5: Tian et al. (2018); 6: W. Yang et al. (2017); 7: Yang (2014); 8: Xu et al. (2015); 9: Zha et al. (2014); 10: Yue et al. (2016); 11: Liu (2017); 12: Yun et al. (2017); 13: Yun (2018).

the emission coefficient K and the observed NO_x concentration (Cui et al., 2018; Huang et al., 2017) (see Eq. 1). Since it is difficult to determine the time of NO_x emissions, method (1) can not exclude the NO_x levels before emission begins. With this in mind, in method (2), the primary emission rate P_{emis} is estimated as the product of the emission coefficient K and $[\Delta NO_x]/\Delta t$, where $[\Delta NO_x]$ is the difference between the NO_x observed at two time points (Liu et al., 2019b; Zheng et al., 2020) (see Eq. 2). Obviously, this can only be used when NO_x is increasing. It should be noted that any loss of NO_x and HONO can be a source of error in these two methods, especially during the daytime. In method (3), the primary emission rate P_{emis} is equal to the product of the emission coefficient K and NO_x^*, the NO_x emission from the source emission inventory (Michoud et al., 2014; Su et al., 2008b) (see Eq. 3). This method adheres to the definition of the HONO emission rate which assumes that the primary sources are evenly mixed in a specific area. It is desirable to use emission inventory data with high spatial and temporal resolution to obtain an accurate estimate.

$$[HONO]_{emis} = K \times [NO_x] \quad (1)$$

$$P_{emis} = K \times [\Delta NO_x]/\Delta t \quad (2)$$

$$P_{emis} = K \times NO_x^* \quad (3)$$

$$P_{HONO} = \frac{[HONO]_{t_2} - [HONO]_{t_1}}{t_2 - t_1} \quad (4)$$

In this study, we first used the NO_x emission rate from a high-resolution emission inventory (Huang et al., 2021) to calculate the emission rate of HONO P_{emis} at night (18:00–06:00). The NO_x emission rate was extracted from a 3 km × 3 km grid cell centered around our site. As a comparison, we also used the 2017 NO_x emission inventory of Guangzhou City to repeat the calculation. The two inventories primarily differ in their spatial resolutions. The high-resolution 3 km × 3 km data are expected to better represent local traffic emissions, whereas the city-level emission inventory represents the total emissions. Since we cannot quantify the relative contribution of the local and regional emissions to this site, two results are used to represent the upper and lower limits of the contribution of primary emissions to the HONO production. The nighttime height of the boundary layer is assuming to 200 m, based on a previous study of the PRD region in autumn by Fan et al. (2008).

The observed HONO accumulation rate P_{HONO} is calculated using Eq. (4), where $[HONO]_{t_1}$ and $[HONO]_{t_2}$ represent the HONO concentrations at 18:00 and 06:00 LT, respectively. An average P_{HONO} of 0.02 ± 0.06 ppbv h^{-1} can then be derived. The hourly HONO primary emission rates calculated with the two inventories are shown in Fig. 5a. P_{emis} calculated with the high-resolution emission data (3 km × 3 km) shows a steep downward trend from 18:00 (0.56 ppbv h^{-1}) to 04:00 (0.14 ppbv h^{-1}) followed by an upward trend from

04:00 (0.14 ppbv h^{-1}) to 06:00 (0.25 ppbv h^{-1}), with an average of 0.30 ± 0.15 ppbv h^{-1}. By contrast, the P_{emis} obtained with the city-level emission data (Guangzhou) is much lower (0.04 ± 0.02 ppbv h^{-1}) and varied smoothly throughout the night. Similar results have been obtained at urban sites (Liu et al., 2020a, b; Gu et al., 2021) and a suburban site (Michoud et al., 2014) but a much lower result was obtained at a rural site (Su et al., 2008b) in the PRD region. The uncertainty of P_{emis} stems from the uncertainty of the inventories (−25 % to 28 %) (Huang et al., 2021). Regardless, direct emission of HONO represents a large HONO source at night, along with other sources of HONO that remain to be considered.

We also calculated the contribution of primary emissions to the HONO concentration ($[HONO]_{emis}/[HONO]$) using Method (1) and made comparisons with $[HONO]_{emis}/[HONO]$ ratios obtained previously from urban sites in China (Table S3). The values varied widely from 12 % to 52 %, with seasonal differences of more than a factor of 2 for the same site, reflecting a large variability of HONO emissions spatially and temporally. In comparison, the ratio $[HONO]_{emis}/[HONO]$ at our site is relatively high at 47 %, as can be expected from the relatively strong vehicle exhaust emissions near our site.

In addition to traffic emissions, we also estimated the HONO emission rate from soil P_{soil} (ppbv h^{-1}) according to Eq. (5) (Liu et al., 2020a):

$$P_{soil} = \frac{\alpha F_{soil}}{H}, \quad (5)$$

where F_{soil} is the emission flux (g m^{-2} s^{-1}); H is the height of the boundary layer (m), assumed to be 200 m (Fan et al., 2008); α is the conversion factor ($\alpha = \frac{1\times10^9\times3600\times R\times T}{M\times P} = \frac{2.99\times10^{13}\times T}{M\times P}$); T is the temperature (K); M is the molecular weight (g mol^{-1}); and P is the atmospheric pressure (Pa). The HONO emission flux from soil depends on the temperature, water content, and nitrogen nutrient content of soil, which were considered here using parameters reported in the literature (Oswald et al., 2013). Since grassland, coniferous forest, and tropical rain forest are the typical plants in the Guangzhou City area (Wu et al., 2015) and their emission fluxes are comparable (Oswald et al., 2013), the emission flux from grassland was adopted to represent the soil HONO emission in Guangzhou. The average nighttime P_{soil} varied from 0.011 to 0.035 ppbv h^{-1}, with a mean value of 0.019 ± 0.009 ppbv h^{-1}. The HONO emission rate from soil at our site is slightly larger than the result reported in the Shijiangzhuang urban area (Liu et al., 2020a) and comparable to that in the Beijing urban area (Liu et al., 2020b). A caveat is that the calculation relies on laboratory results and is therefore prone to errors due to any possible inconsistency between laboratory simulations and field observations. Overall, soil emission is a minor source compared to other sources.

3.2.2 Homogeneous NO + OH reaction

The reaction between NO and OH is the most well-known homogeneous HONO source. It can contribute a substantial fraction of the HONO formed when NO and OH concentrations are high (Alicke et al., 2003; Liu et al., 2019b; Wong et al., 2011; Tong et al., 2015; Zhang et al., 2019). Taking the homogeneous Reactions (R2) and (R5) into account, the net HONO homogeneous production rate can be calculated using Eq. (6):

$$HONO + OH \rightarrow NO_2 + H_2O, \quad (R5)$$

$$P^{net}_{OH+NO} = k_{NO+OH}[NO][OH] - k_{HONO+OH}[HONO][OH]. \quad (6)$$

In Eq. (6), k_{NO+OH} (7.2×10^{-12} cm^3 s^{-1}) and $k_{HONO+OH}$ (5.0×10^{-12} cm^3 s^{-1}) are the reaction rate constants of Reactions (R2) and (R5) at 298 K, respectively (Li et al., 2012). Since the OH concentration was not measured, the average nighttime value of 0.5×10^6 cm^{-3} measured in Heshan in the PRD region in the autumn of 2014 was assumed (Tan et al., 2019). As shown in Fig. 3, the variation of P^{net}_{OH+NO} largely followed that of NO, since the concentration of NO was 10 times larger than that of HONO. Also, the average value of P^{net}_{OH+NO} is 0.13 ± 0.30 ppbv h^{-1}, leading to a cumulative HONO contribution of 1.62 ppbv. The obtained P^{net}_{OH+NO} is similar to those in previous studies, such as 0.12 ppbv h^{-1} in Xianyang (Li et al., 2021), 0.13 ppbv h^{-1} in Zhengzhou (Hao et al., 2020), 0.26 ppbv h^{-1} in Xi'an (Huang et al., 2017), and 0.28 ppbv h^{-1} in Guangzhou Back Garden (Li et al., 2012). We note that the measured HONO only increased by 0.26 ppbv in this period, much smaller than the cumulative production of HONO from the reaction between NO and OH, indicating the presence of a large sink to balance this source and other sources that will be discussed below.

Since OH was not measured in our study, we carried out sensitivity tests using one-fifth and twice the assumed OH concentration (0.5×10^6 cm^{-3}) (Lou et al., 2010). As shown in Table S4, within the range of nighttime OH concentrations, the cumulative production from the homogeneous reaction of NO + OH in this study is always large enough to surpass the average measured accumulation of HONO, indicating that the NO + OH source is a major source term regardless of uncertainties in OH concentrations.

3.2.3 Heterogeneous NO_2 to HONO conversion

Our analysis so far suggests that direct emissions and the homogeneous reaction between NO and OH are two major sources of HONO at night. This finding is in line with the relatively high correlation ($R^2 = 0.5927$) between HONO and NO (Fig. 4a). In the following, we present results from correlation analysis to explore possible pathways for heterogeneous NO_2 to HONO conversion at night (18:00–06:00).

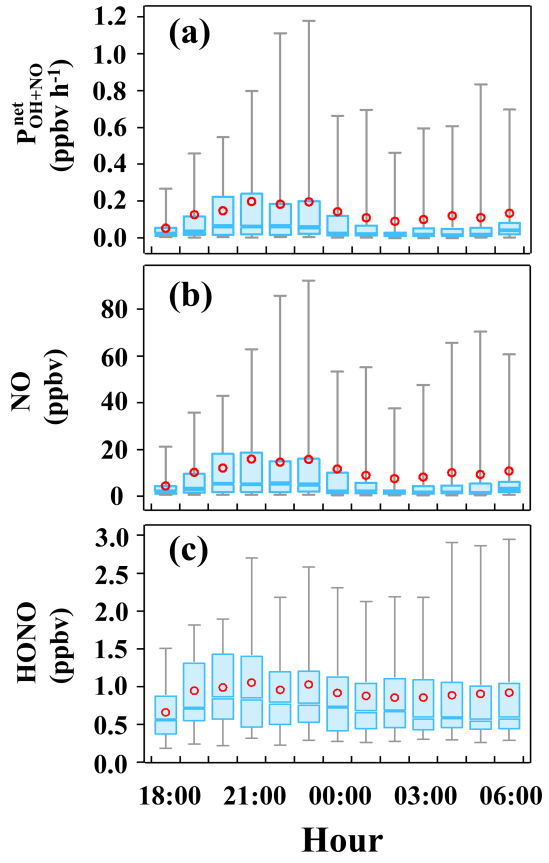

Figure 3. The mean nocturnal variations of **(a)** P^{net}_{OH+NO}, **(b)** NO, and **(c)** HONO. In each box, the blue line and red circle refer to the median and mean, respectively. The upper and lower boundaries in each box represent the 75th and the 25th percentiles; the whiskers above and below each box represent the 95th and 5th percentiles.

The ratio HONO/NO_2 has often been used to indicate the heterogeneous conversion efficiency of NO_2 to HONO (Lammel and Cape, 1996; Stutz et al., 2002), as it is less influenced by transport processes or convection. Figure 4c shows a weak correlation ($R^2 = 0.0638$) between HONO/NO_2 and $PM_{2.5}$, suggesting that the formation of HONO on aerosol surfaces might not be the main pathway (Kalberer et al., 1999; Kleffmann et al., 2003; Wong et al., 2011; Zhang et al., 2009; Sörgel et al., 2011a; VandenBoer et al., 2013). Because the surface area of the ground (including vegetation surfaces, building surfaces, soil, etc.) is generally larger than the surface area of aerosols, some studies have suggested that the heterogeneous reaction of NO_2 and water vapor on ground surfaces is the main source of HONO (Harrison and Kitto, 1994; Li et al., 2012; Wong et al., 2012). Furthermore, the correlations between HONO/NO_2 and NH_3 and RH are 0.3746 and 0.2381, respectively, and the correlation between HONO/NO_2 and the product of NH_3 and RH is even stronger ($R^2 = 0.4597$). Some studies have proposed that NH_3 can decrease the free-energy barrier in the hydrolysis of NO_2, thus enhancing HONO formation (Xu et al., 2019; L. Li et al., 2018; G. Wang et al., 2021).

In Fig. S5, we further explore the RH effect by focusing on high HONO/NO_2 values, i.e., the five highest HONO/NO_2 values in 5 % RH intervals (Stutz et al., 2004). When RH was lower than 87.5 %, HONO/NO_2 increased with RH, which is in accordance with the reaction kinetics of the disproportionation reaction of NO_2 and H_2O. Furthermore, the slope of the linear fit between HONO/NO_2 and RH was much smaller in the RH range of 30 %–70 % (slope = 0.04 %; $R^2 = 0.5202$) than in the RH range of 70 %–87.5 % (slope = 0.25 %, $R^2 = 0.8767$). Similar piecewise correlations between HONO/NO_2 and RH have been found in previous studies (Qin et al., 2009; Zhang et al., 2019), which have been interpreted as evidence for the nonlinear dependence of the NO_2-to-HONO conversion efficiency on RH. Once the relative humidity exceeded 87.5 %, NO_2-to-HONO conversion appeared to be inhibited by the RH (slope = −0.32 %; $R^2 = 0.9750$). A possible explanation is that the number of water layers formed on various surfaces increased rapidly with RH, resulting in effective uptake of HONO and making the surface inaccessible or less reactive to NO_2. Previous studies also found fast growth of aqueous layers when RH was over 70 % for glass (Saliba et al., 2001) and when it was over 80 % for stone (Stutz et al., 2004). The tipping point inferred from ambient observations appears to vary depending on the locale (likely reflecting the different compositions of the ground surfaces), e.g., 60 % for Chengdu (Y. Yang et al., 2021), 65 %–70 % for Beijing (J. Wang et al., 2017), 70 % for Back Garden (Li et al., 2012), 75 % for Shanghai (Wang et al., 2013), and 85 % for Xi'an (Huang et al., 2017).

We calculated the strength of HONO formation from the heterogeneous reaction of NO_2 on the ground surface (P_{ground}) and on the aerosol surface ($P_{aerosol}$) based on empirical data derived from either experiments or observations:

$$P_{ground} = \frac{1}{8}\gamma_{NO_2\rightarrow ground} \times [NO_2] \times C_{NO_2} \times \frac{S_g}{V}, \quad (7)$$

$$P_{aerosol} = \frac{1}{4}\gamma_{NO_2\rightarrow aerosol} \times [NO_2] \times C_{NO_2} \times \frac{S_a}{V}, \quad (8)$$

$$\frac{S_g}{V} = \frac{2.2}{H}, \quad (9)$$

where C_{NO_2} is the mean molecular velocity of NO_2 (m s^{-1}), $\gamma_{NO_2\rightarrow ground}$ and $\gamma_{NO_2\rightarrow aerosol}$ represent the uptake coefficients of NO_2 on the ground surface and aerosol surface, respectively, while S_g/V and S_a/V are the surface area to volume ratios (m^{-1}) for both the ground and aerosol, respectively. Considering the land-use type of the study site, we treated the ground as an uneven surface, and a factor of 2.2 per unit of ground surface, as measured by Voogt and Oke (1997), was adopted to calculate the total active surface. Hence, S_g/V can be calculated by Eq. (9), where H is the mixing layer height. The surface area to volume ratio S_a/V

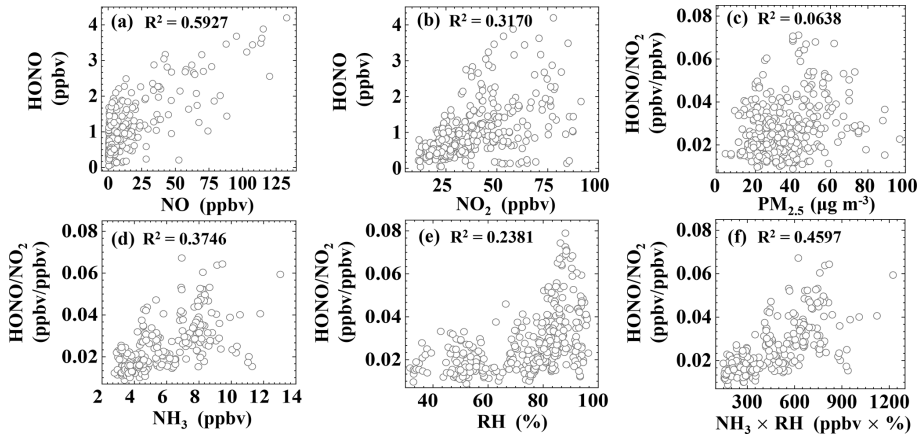

Figure 4. Correlations between HONO, $HONO/NO_2$, and various parameters during the time interval of 18:00–06:00.

of PM_{10} was not available in this study and was estimated according to the $PM_{2.5}$ and S_a/V values in Guangzhou Xinken reported by Su et al. (2008a). The uptake coefficients of NO_2 on the ground surface and aerosol surface were assumed to be 4×10^{-6} following previous studies (D. Li et al., 2018; Liu et al., 2019a; Zhang et al., 2021) (a summary of the parameterizations used for nighttime HONO budget calculation can be found in Table S5). With these assumptions, an average value of P_{ground} of 0.27 ± 0.13 ppbv h^{-1} can be derived, which is far larger than $P_{aerosol}$ (0.03 ± 0.02 ppbv h^{-1}) (Fig. 5c and d).

In sum, our correlation analysis for $HONO/NO_2$ and parameterized calculations suggested that nighttime heterogeneous conversion of NO_2 into HONO at our site mainly occurred on the ground rather than on aerosol sources, while correlation analysis provides evidence for the roles of NH_3 and water vapor in HONO formation. It should be noted that, unlike the NO + OH reaction or primary emission, which were found to be major HONO sources even at their lower limits considering uncertainties, the magnitude of the heterogeneous source as well as its contribution to the overall HONO budget varied greatly with the assumed uptake coefficients of NO_2, which can span two orders of magnitude.

3.2.4 Removal of HONO

As discussed above, strong sinks are required to balance the nighttime HONO production. Since the reactions of HONO + OH and HONO + HONO are negligible (Kaiser and Wu, 1977; Mebel et al., 1998), it is conceivable that nighttime HONO is mainly removed through deposition L_{Dep} (El Zein and Bedjanian, 2012; Li et al., 2012; Hao et al., 2020; Meng et al., 2020), transport processes, e.g., entrainment of background air $L_{dilution}$ (Gall et al., 2016; Meng et al., 2020), and uptake on aerosols $L_{aerosol}$. These terms can be expressed as follows:

$$L_{Dep} = \frac{V_d \times [HONO]}{H}, \quad (10)$$

$$L_{aerosol} = \frac{1}{4}\gamma_{HONO \rightarrow aerosol} \times [HONO] \times C_{HONO} \times \frac{S_a}{V}, \quad (11)$$

$$L_{dilution} = k_{(dilution)} \times \left([HONO] - [HONO]_{background}\right), \quad (12)$$

where V_d is the average deposition velocity, $\gamma_{HONO \rightarrow aerosol}$ is the uptake coefficient of HONO on the aerosol surface, and $k_{(dilution)}$ is the dilution rate (including both vertical and horizontal transport) (Dillon et al., 2002). C_{HONO} is the mean molecular velocity of HONO ($m\,s^{-1}$), and [HONO] and $[HONO]_{background}$ represent the HONO concentrations at the observation site and the background site, respectively. In this work, the lowest nighttime HONO concentration was taken as the $[HONO]_{background}$.

The average loss rate of HONO by dilution was calculated to be 0.18 ± 0.16 ppbv h^{-1}, which is in the range of prior results (Gall et al., 2016; Liu et al., 2020a, b). The average values of $L_{aerosol}$ and $L_{OH+HONO}$ were 0.008 ± 0.006 and 0.008 ± 0.012 ppbv h^{-1}, respectively. In order to balance the nighttime HONO budget, and assuming dry deposition to be responsible for the remaining amount of HONO loss, a dry deposition rate of ~ 2.5 cm s^{-1} was adopted, accounting for an average loss rate of 0.41 ± 0.31 ppbv h^{-1} by deposition between 18:00–06:00, when using the median parameter values in Table S5 to calculate the HONO sources and sinks. This result is consistent with previous studies suggesting dry deposition as the dominant loss pathway for HONO during the night (Li et al., 2012; Hao et al., 2020; Meng et al., 2020; VandenBoer et al., 2013). The upper limit of $L_{aerosol}$ is only 0.10 ± 0.08 ppbv h^{-1}, suggesting that the HONO loss on aerosols was not a major sink, as also suggested by prior studies (El Zein and Bedjanian, 2012; El Zein et al., 2013; Romanias et al., 2012).

3.2.5 Nighttime HONO budget: relative importance of sources and their uncertainties

It is useful to evaluate the balance of the HONO budget by evaluating calculated/parameterized sources and sinks

against the observed HONO level and variability. The observed production rate of HONO P_{obs} can be defined as the sum of the total loss rates and change rates of HONO (Gu et al., 2021). When using the median values of parameters (Table S5) and taking the average throughout the night (18:00–06:00), all five sources are greater than or close to the average accumulation rate of HONO at night derived from the observed HONO variation (0.02 ± 0.06 ppbv h^{-1}), indicating a balanced HONO budget considering all uncertainties. Ranking the source strengths with their median estimates suggested that heterogeneous conversion of NO_2 on the ground surface (0.27 ± 0.13 ppbv h^{-1}), primary emission from vehicle exhaust (between 0.04 ± 0.02 and 0.30 ± 0.15 ppbv h^{-1}, with a middle value of 0.16 ± 0.07 ppbv h^{-1}), and the homogeneous reaction of NO + OH (0.14 ± 0.30 ppbv h^{-1}) were major sources of HONO at night. The nighttime soil emission rate (0.019 ± 0.009 ppbv h^{-1}) and heterogeneous NO_2 conversion on the aerosol surfaces (0.03 ± 0.02 ppbv h^{-1}) were two other minor sources. Dry deposition (0.41 ± 0.31 ppbv h^{-1}) was the principal loss process of nighttime HONO, followed by dilution (0.18 ± 0.16 ppbv h^{-1}), while the homogeneous reaction of HONO + OH (0.008 ± 0.012 ppbv h^{-1}) and HONO uptake on the aerosol surfaces (0.008 ± 0.006 ppbv h^{-1}) were insignificant.

We also made an attempt to obtain a time-resolved HONO budget on an hourly basis, although the results are not satisfactory for all the hours at night, with obvious differences seen between observed and calculated rates of HONO variation, e.g., at 22:00 and from 02:00 to 05:00 (Fig. S6). This is expected considering the much more amplified uncertainties associated with the hourly variabilities of various quantities, which can be considerably reduced by averaging all hours. This is why subtle and careful data filtering is necessary when nighttime HONO chemistry is examined in detail (Wong et al., 2011). Such a granular analysis is more appropriate for the daytime, when the HONO lifetime is much shorter and uncertainties affecting the interpretation of HONO chemistry (e.g., emission and transport) are much more muted. As a matter of fact, because the rate of HONO change shown in Fig. S6 is a first-order derivative of the HONO concentration itself, one would expect that HONO concentrations from each source would show greater variations, making it more difficult to compare on an hourly basis. Another challenge is that since the parameters used for calculating HONO source strengths have ranges for their estimates (Table S5), the HONO source strengths also have a wide range individually, and therefore there are numerous possible combinations of these sources with different strengths and rankings to close the budget.

The comparison and ranking of sources considering variability and uncertainty is less straightforward than ranking the nighttime average source strengths (Fig. 5). Among the three largest sources, both primary (non-soil) emission and the NO_2 heterogeneous source on the ground showed an evening peak and decreased after midnight. The NO + OH source showed a different trend, with its lowest level occurring in the evening, making it the smallest source among the three at that time. Although the NO_2 heterogeneous source on the ground appeared to be the largest based on its median parameter value, it also had the largest range of estimates, suggesting that its importance is more uncertain compared to the other sources. On the other hand, the other two minor sources, i.e., the NO_2 heterogeneous source on aerosols and soil emission, are substantially less important than these three sources given their ranges of low estimates. The variability and uncertainty of dry deposition are entirely dependent on other terms of sources and sinks, since it is derived as a final term to balance the budget.

3.3 Daytime HONO budget and unknown sources analysis

3.3.1 Budget analysis

In this section, we move on to a detailed budget analysis for HONO during the daytime, when the chemistry is distinctly different from that at night. Similar to the nighttime analysis, by exploring different terms for the daytime chemistry, the time variation of the HONO concentration at our site can be related to its sources and sinks as follows:

$$\begin{aligned}\frac{\partial[\mathrm{HONO}]}{\partial t} &= P_{\mathrm{HONO}} - L_{\mathrm{HONO}} \\ &= (P_{\mathrm{OH+NO}} + P_{\mathrm{Unknown}} + P_{\mathrm{emis}} + P_{\mathrm{soil}} \\ &\quad + T_{\mathrm{V}} + T_{\mathrm{H}}) - (L_{\mathrm{OH+HONO}} + L_{\mathrm{Phot}} + L_{\mathrm{Dep}}), \end{aligned} \quad (13)$$

where $\partial[\mathrm{HONO}]/\partial t$ represents the time variation of HONO; P_{HONO} and L_{HONO} are the sources and sinks of HONO, respectively; $P_{\mathrm{OH+NO}}$ and $L_{\mathrm{OH+HONO}}$ are the homogeneous HONO formation and loss rates in Reactions (R2) and (R5), respectively; P_{Unknown} is the HONO production rate from unknown sources; T_{V} and T_{H} are two terms representing vertical and horizontal transport processes, respectively; L_{Phot} denotes the photolysis loss rate of HONO, which can be calculated as $L_{\mathrm{Phot}} = J(\mathrm{HONO}) \times [\mathrm{HONO}]$; and the deposition loss rate of HONO L_{Dep} can be calculated using Eq. (10). Assuming a daytime V_{d} of 1.6 cm s^{-1} (Hou et al., 2016; Li et al., 2011) and a daytime mixing height (H) of 1000 m (Liao et al., 2018; Song et al., 2019), the average L_{Dep} is 0.003 ± 0.001 ppbv h^{-1}, which is three orders of magnitude smaller than L_{Phot} and can therefore be ignored in the following discussion.

OH was not measured; it was calculated with a parameterized approach based on the strong correlation between observed OH radicals and $J(\mathrm{O}^1\mathrm{D})$. The parameterization was first proposed by Rohrer and Berresheim (2006) and has been applied in several studies in China (Lu et al., 2013, 2012, 2014). In this study, OH was estimated with the observed $J(\mathrm{O}^1\mathrm{D})$ along with parameters obtained by fitting the observed OH radicals and $J(\mathrm{O}^1\mathrm{D})$ data for Guangzhou

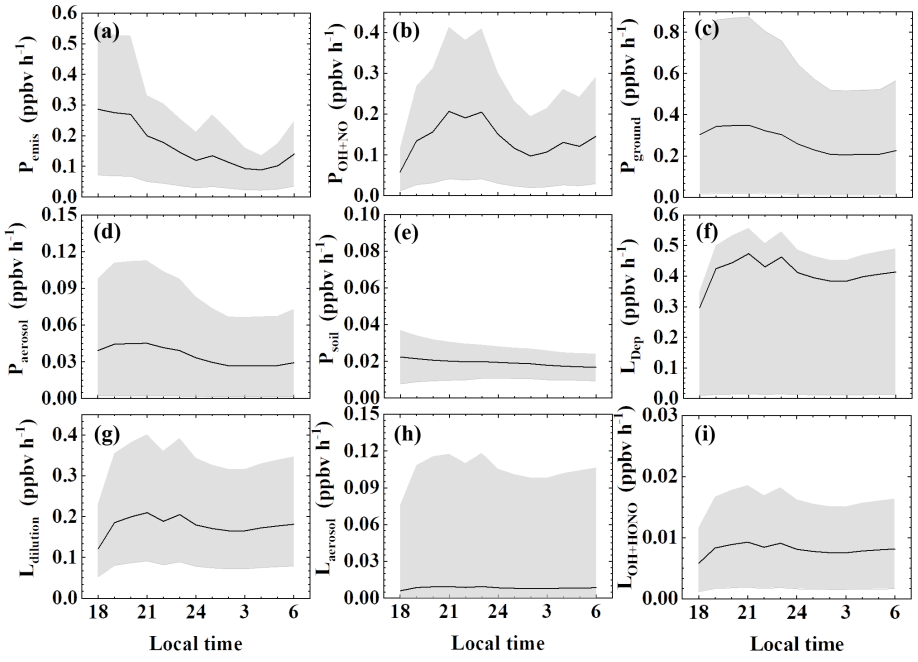

Figure 5. Nocturnal variations of the terms in the HONO budget: **(a)** primary emission from vehicle exhaust, **(b)** homogeneous reaction of NO + OH, **(c)** heterogeneous conversion of NO_2 on ground surfaces, **(d)** heterogeneous conversion of NO_2 on aerosol surfaces, **(e)** soil emission, and HONO losses from **(f)** dry deposition, **(g)** dilution, **(h)** uptake on aerosols, and **(i)** HONO + OH during 27 September–9 November 2018 in Guangzhou. In each plot, the black line is the HONO production rate with the median parameter value, and the gray shadow represents their lower and upper limits.

Back Garden from Lu et al. (2012). The daytime maximum OH concentration was estimated to be 1.3×10^7 cm^{-3}, which is slightly smaller than the daily peak values of 1.5–2.6 $\times 10^7$ cm^{-3} observed in the summer in Guangzhou by Lu et al. (2012). Also, the estimated daily average OH concentration is 6.7×10^6 cm^{-3}, close to the value of 7.5×10^6 cm^{-3} measured in the PRD region in the autumn of 2014 by Y. Yang et al. (2017). The daytime P_{emis} was calculated based on method (3) (mentioned in Sect. 3.2.1). Because the HONO lifetime was of the order of 20 min under typical daytime conditions (Stutz et al., 2000) and the transport distance is only a few kilometers, the NO_x emission rate extracted from the 3 km × 3 km grid cell centered around the sampling site was used to calculate the impact of primary emission on HONO.

To minimize interferences, we chose the period from 09:00 to 15:00, with intense solar radiation and a short HONO lifetime. The horizontal transport T_H was assumed negligible, as cases with low wind speeds (below 3 m s^{-1}) were selected (Su et al., 2008b; Yang et al., 2014). The magnitude of the vertical transport T_V can be estimated by using a parameterization for dilution by background air according to Dillon et al. (2002), i.e., $T_V = k_{(dilution)} \times ([HONO] - [HONO]_{background})$, where $k_{(dilution)}$ is the dilution rate and $[HONO]_{background}$ represents the background HONO concentration. Assuming a $k_{(dilution)}$ of 0.23 h^{-1} (Dillon et al., 2002; Sörgel et al., 2011a) and a $[HONO]_{background}$ value of 10 pptv (Zhang et al., 2009), and taking the mean noontime [HONO] value of 400 pptv in this study, a value of about 0.09 ppbv h^{-1} can be derived, which is much smaller than L_{Phot} and can be ignored in the following discussion. The average daytime HONO emission rate from soil P_{soil} varied from 0.002 to 0.007 with a mean value of 0.004 ± 0.002 ppbv h^{-1}, which is three orders of magnitude smaller than L_{Phot} and can also be ignored in the following discussion. As a result, $P_{Unknown}$ can be expressed by Eq. (14), in which $\partial[HONO]/\partial t$ is substituted by $\Delta[HONO]/\Delta t$.

$$\frac{\Delta[HONO]}{\Delta t} = (P_{OH+NO} + P_{emis} + P_{Unknown}) - (L_{OH+HONO} + L_{Phot}) \quad (14)$$

Figure 6 shows the budget of HONO from 09:00 to 15:00. As expected, photolysis HONO loss was the main loss pathway in the day (L_{Phot} was 1.58 ± 0.82 ppbv h^{-1}), followed by a small contribution from the homogeneous reaction of HONO + OH ($L_{OH+HONO}$, 0.07 ± 0.03 ppbv h^{-1}). Among the sources, P_{OH+NO} and $P_{Unknown}$ were comparable in magnitude, with an average of 0.79 ± 0.61 and 0.65 ± 0.46 ppbv h^{-1}, respectively. $P_{Unknown}$ showed a photoenhanced feature, reaching its maximum at 12:00 at 0.97 ppbv h^{-1}, similar to observations in Xinken (Su et al., 2008b), Beijing (Yang et al., 2014), Wangdu (Liu et al., 2019a), Changzhou (Zheng et al., 2020), and Cyprus

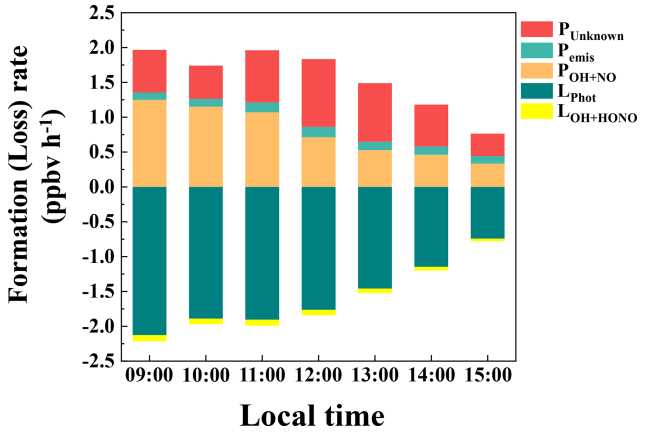

Figure 6. Items in the HONO budget (Eq. 14) for Guangzhou during the observation period.

(Meusel et al., 2016). The average of P_{Unknown} is comparable to that observed in Back Garden (0.77 ppbv h^{-1}) by Li et al. (2012), but smaller than those found in Xinken ($\approx$ 2.0 ppbv h^{-1}) by Su et al. (2008b) and the Guangzhou City area (1.25 ppbv h^{-1}) by W. Yang et al. (2017). The homogeneous reaction of NO + OH reached its maximum in the early morning and contributed the largest fraction during the whole day. Apparently, high NO concentrations at our site made $P_{\text{OH+NO}}$ the biggest daytime source of HONO, exceeding P_{Unknown}, similar to observations at other high-NO_x sites such as the Uintah Basin (Tsai et al., 2018), Houston (Wong et al., 2013), Denver (VandenBoer et al., 2013), Santiago de Chile (Elshorbany et al., 2009), London (Heard et al., 2004), Paris (Michoud et al., 2014), Beijing (Liu et al., 2021; Slater et al., 2020; Zhang et al., 2019; Liu et al., 2020b), Hebei (Xue et al., 2020), and Taiwan (Lin et al., 2006). Next, we investigate possible factors relating to P_{Unknown}.

3.3.2 Possible mechanisms for daytime HONO production

Figure 7 shows that the correlations of P_{Unknown} with NO_2 and $J(NO_2)$ were 0.0681 and 0.2713, respectively, while the correlation between P_{Unknown} and $NO_2 \times J(NO_2)$ was greater: 0.4116, indicating that P_{Unknown} may be related to the photoenhanced reaction of NO_2 (Jiang et al., 2020; D. Li et al., 2018; Liu et al., 2019a, b; Su et al., 2008b; Zheng et al., 2020; Huang et al., 2017). No correlation was found between P_{Unknown} and $PM_{2.5}$ ($R^2 = 0.0001$), indicating that particulate matter may not be a key factor in daytime HONO production (Wong et al., 2012; D. Li et al., 2018; Sörgel et al., 2011a; J. Wang et al., 2017; Zheng et al., 2020). Meanwhile, the correlations of P_{Unknown} with nitrate in PM_1 and the sum of gaseous nitric acid and nitrate in PM_1 were very low, with R^2 values of 0.0348 and 0.0062, respectively. The correlation between P_{Unknown} and the product of nitrate and $J(NO_2)$ was also poor ($R^2 = 0.0073$), indicating that P_{Unknown} was not related to the photolysis of nitrate or gaseous nitric acid. Wang et al. (2016) and Ge et al. (2019) suggested that NH_3 can efficiently promote the reaction of NO_2 and SO_2 to form HONO and sulfate. However, we did not find good correlations of P_{Unknown} vs. NH_3, P_{Unknown} vs. SO_2, or P_{Unknown} vs. $NH_3 \times SO_2$.

In summary, at our site with a relatively strong traffic impact and high NO, NO + OH appears to be the largest daytime HONO source, followed by an unknown photolytic source that does not seem to be related to aerosols, nor the photolysis of nitrate/nitric acid, nor the reaction between NO_2, SO_2, and NH_3.

4 Conclusions

Nitrous acid (HONO) was measured with a custom-built LOPAP instrument, along with meteorological parameters and other atmospheric constituents, at an urban site in Guangzhou in the Pearl River Delta from 27 September to 9 November 2018. The HONO concentrations varied from 0.02 to 4.43 ppbv with an average of 0.74 ± 0.70 ppbv. Compared to prior measurements in Guangzhou, a decreasing trend in HONO can be seen along with improved air quality in the city over the past decade.

We have investigated the budget of HONO at this site using these data, and our key findings are summarized as follows.

We found that the emission ratios ($HONO/NO_x$) derived from an analysis of 11 fresh plumes varied from 0.1 % to 1.5 % with an average value of $0.9\% \pm 0.4\%$. Using this estimated emission ratio and an estimate of the NO_x emission rate extracted from a grid cell around our site in a high-resolution (3 km × 3 km) NO_x emission inventory, we estimated a primary HONO emission rate of 0.30 ± 0.15 ppbv h^{-1}, which turned out to be far larger (by almost an order of magnitude) than what would be estimated with a city-level NO_x emission estimate that does not adequately represent the NO_x emission rate specifically for the observation site. Thus, in future analyses of HONO data, to properly estimate the direct emissions of HONO, we suggest that high-quality emission data should be used to reduce uncertainty. This is especially crucial for a site like ours that receives nearby traffic emissions.

HONO was produced at night at a rate of 0.14 ± 0.30 ppbv h^{-1} by the homogeneous reaction of NO + OH, which represents a secondary HONO source. Another major secondary HONO source at night is the heterogeneous conversion of NO_2 on the ground surface (0.27 ± 0.13 ppbv h^{-1}). Correlation analysis shows that the heterogeneous reaction of NO_2, which is related to NH_3 and the RH, may contribute to nighttime HONO formation. These two secondary sources and the primary emissions from vehicle exhaust (between 0.04 ± 0.02 and 0.30 ± 0.15 ppbv h^{-1}, with a median value

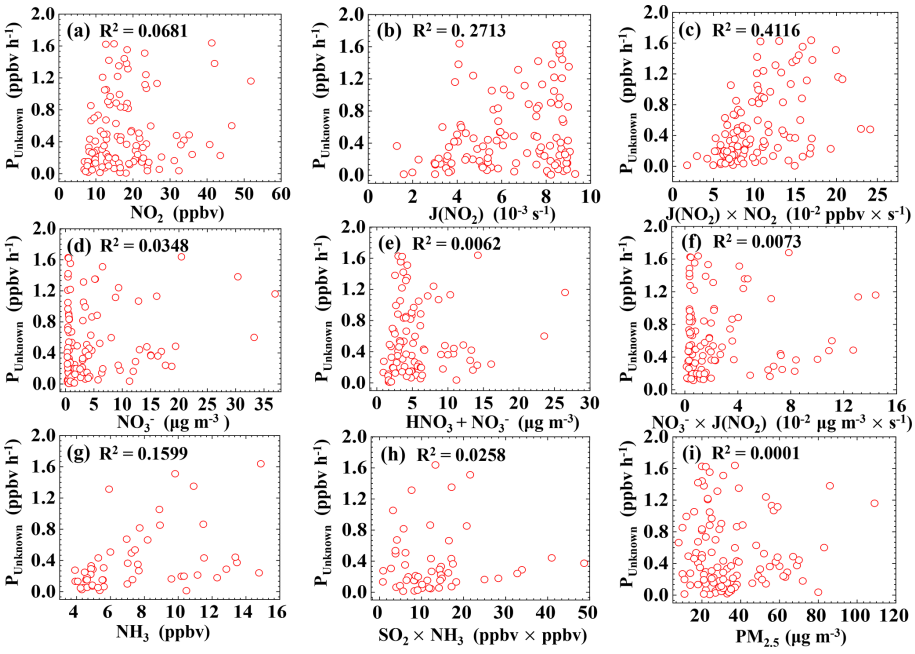

Figure 7. Correlations between the unknown daytime HONO source P_{Unknown} and related parameters.

of 0.16 ± 0.07 ppbv h^{-1}) were found to be the three largest sources of HONO at night. Because of the large ranges assumed for those parameter values when calculating them (e.g., the NO_2 uptake coefficient, which spans two orders of magnitude), the relative importance of the three major sources depends on these assumptions. Soil emission (0.019 ± 0.009 ppbv h^{-1}) and heterogeneous NO_2 conversion on aerosol surfaces (0.03 ± 0.02 ppbv h^{-1}) were two other minor sources. Our calculations suggested that dilution acted as a major sink (0.18 ± 0.16 ppbv h^{-1}), while the loss of HONO on aerosol surfaces played a much less important role. In order to balance the nighttime HONO budget, and assuming dry deposition to be responsible for the remaining amount of HONO loss, a dry deposition rate of 2.5 cm s^{-1} is required, equivalent to a loss rate of 0.41 ± 0.31 ppbv h^{-1}.

Daytime HONO budget analysis revealed that in order to sustain the observed HONO concentration at around 450 pptv despite the fast photolysis of HONO, an additional unknown source production rate (P_{Unknown}) of 0.65 ± 0.46 ppbv h^{-1} was needed in addition to the primary emission P_{emis} of 0.12 ± 0.02 ppbv h^{-1} and the homogeneous reaction source $P_{\mathrm{OH+NO}}$ of 0.79 ± 0.61 ppbv h^{-1}. It is worth noting that the homogeneous HONO source from NO + OH appeared to be a stronger source of HONO than the unknown source (P_{Unknown}), because of the high levels of NO at our site. Correlation analysis between P_{Unknown} and proxies for different mechanisms showed that P_{Unknown} appears to have been photoenhanced, but the mechanism remains unclear. As suggested by the weak correlation between P_{Unknown} and $PM_{2.5}$, aerosols did not appear to be as important a heterogeneous reaction medium as the ground. No correlations were found between P_{Unknown} and nitrate or HNO_3, NH_3, and SO_2.

Overall, these results from our study offer a unique perspective on the HONO at an urban site receiving heavy traffic emissions in the PRD region. Our budget calculations and comprehensive uncertainty analysis suggest that at such locations as ours, direct HONO emissions and NO + OH can become comparable to or even surpass other HONO sources that typically receive greater attention and interest, such as the NO_2 heterogeneous source and the unknown daytime photolytic source. Our findings emphasize the need to reduce the uncertainties of both conventional and novel HONO sources and sinks to advance our understanding of this important source of atmospheric OH.

Data availability. The data used in this study are available from the corresponding author upon request (chengp@jnu.edu.cn).

Supplement. The supplement related to this article is available online at: https://doi.org/10.5194/acp-22-8951-2022-supplement.

Author contributions. PC organized the field campaign. YY and HL analyzed the data and wrote the paper. All authors contributed to measurements, discussed results, and commented on the paper. YY and PC contributed equally to this work. WY, BH and XY maintained the custom-built LOPAP and processed the data. WS provided the meteorological data. WH provided the gaseous HNO_3 and particulate nitrate data. XW provided the commercial LOPAP data. BY and MS provided the photolysis frequencies data. ZH, ZL

and JZ provided the high-resolution NO_x emission inventory. HW gave valuable comments on this paper.

Competing interests. The contact author has declared that neither they nor their co-authors have any competing interests.

Disclaimer. Publisher's note: Copernicus Publications remains neutral with regard to jurisdictional claims in published maps and institutional affiliations.

Acknowledgements. We thank Jörg Kleffmann for his comments and suggestions. We also thank the anonymous referees and the editor, Steven Brown, for their insightful and constructive comments, which helped in improving the paper.

Financial support. This research has been supported by the National Key Research and Development Program of China (grant nos. 2018YFC0213904, 2017YFC0210104), Science and Technology Plan Projects in Guangzhou (grant no. 201804010115), the Guangdong Natural Science Funds for Distinguished Young Scholars (grant no. 2018B030306037), the Guangdong Innovative and Entrepreneurial Research Team Program (grant no. 2016ZT06N263), and the Special Fund Project for Science and Technology Innovation Strategy of Guangdong Province (grant no. 2019B121205004).

Review statement. This paper was edited by Steven Brown and reviewed by two anonymous referees.

References

Acker, K., Spindler, G., and Brüggemann, E.: Nitrous and nitric acid measurements during the INTERCOMP2000 campaign in Melpitz, Atmos. Environ., 38, 6497–6505, https://doi.org/10.1016/j.atmosenv.2004.08.030, 2004.

Acker, K., Febo, A., Trick, S., Perrino, C., Bruno, P., Wiesen, P., Möller, D., Wieprecht, W., Auel, R., Giusto, M., Geyer, A., Platt, U., and Allegrini, I.: Nitrous acid in the urban area of Rome, Atmos. Environ., 40, 3123–3133, https://doi.org/10.1016/j.atmosenv.2006.01.028, 2006.

Alicke, B., Geyer, A., Hofzumahaus, A., Holland, F., Konrad, S., Pätz, H. W., Schäfer, J., Stutz, J., Volz-Thomas, A., and Platt, U.: OH formation by HONO photolysis during the BERLIOZ experiment, J. Geophys. Res.-Atmos., 108, 8247, https://doi.org/10.1029/2001JD000579, 2003.

Ammann, M., Kalberer, M., Jost, D. T., Tobler, L., Rössler, E., Piguet, D., Gäggeler, H. W., and Baltensperger, U.: Heterogeneous production of nitrous acid on soot in polluted air masses, Nature, 395, 157–160, https://doi.org/10.1038/25965, 1998.

Aubin, D. G. and Abbatt, J. P. D.: Interaction of NO_2 with Hydrocarbon Soot: Focus on HONO Yield, Surface Modification, and Mechanism, J. Phys. Chem. A, 111, 6263–6273, https://doi.org/10.1021/jp068884h, 2007.

Bejan, I., Abd-el-Aal, Y., Barnes, I., Benter, T., Bohn, B., Wiesen, P., and Kleffmann, J.: The photolysis of ortho-nitrophenols: a new gas phase source of HONO, Phys. Chem. Chem. Phys., 8, 2028–2035, https://doi.org/10.1039/B516590C, 2006.

Chan, C. K. and Yao, X.: Air pollution in mega cities in China, Atmos. Environ., 42, 1–42, https://doi.org/10.1016/j.atmosenv.2007.09.003, 2008.

Colussi, A. J., Enami, S., Yabushita, A., Hoffmann, M. R., Liu, W.-G., Mishra, H., and Goddard, I. I. I. W. A.: Tropospheric aerosol as a reactive intermediate, Faraday Discuss., 165, 407–420, https://doi.org/10.1039/C3FD00040K, 2013.

Cui, L., Li, R., Zhang, Y., Meng, Y., Fu, H., and Chen, J.: An observational study of nitrous acid (HONO) in Shanghai, China: The aerosol impact on HONO formation during the haze episodes, Sci. Total Environ., 630, 1057–1070, https://doi.org/10.1016/j.scitotenv.2018.02.063, 2018.

Dillon, M. B., Lamanna, M. S., Schade, G. W., Goldstein, A. H., and Cohen, R. C.: Chemical evolution of the Sacramento urban plume: Transport and oxidation, J. Geophys. Res.-Atmos., 107, ACH 3-1–ACH 3-15, https://doi.org/10.1029/2001JD000969, 2002.

Elshorbany, Y. F., Kurtenbach, R., Wiesen, P., Lissi, E., Rubio, M., Villena, G., Gramsch, E., Rickard, A. R., Pilling, M. J., and Kleffmann, J.: Oxidation capacity of the city air of Santiago, Chile, Atmos. Chem. Phys., 9, 2257–2273, https://doi.org/10.5194/acp-9-2257-2009, 2009.

El Zein, A. and Bedjanian, Y.: Reactive Uptake of HONO to TiO_2 Surface: "Dark" Reaction, J. Phys. Chem. A, 116, 3665–3672, https://doi.org/10.1021/jp300859w, 2012.

El Zein, A., Romanias, M. N., and Bedjanian, Y.: Kinetics and Products of Heterogeneous Reaction of HONO with Fe_2O_3 and Arizona Test Dust, Environ. Sci. Technol., 47, 6325–6331, https://doi.org/10.1021/es400794c, 2013.

Fan, S., Wang, B., Tesche, M., Engelmann, R., Althausen, A., Liu, J., Zhu, W., Fan, Q., Li, M., Ta, N., Song, L., and Leong, K.: Meteorological conditions and structures of atmospheric boundary layer in October 2004 over Pearl River Delta area, Atmos. Environ., 42, 6174–6186, https://doi.org/10.1016/j.atmosenv.2008.01.067, 2008.

Febo, A., Perrino, C., and Allegrini, I.: Measurement of nitrous acid in milan, italy, by doas and diffusion denuders, Atmos. Environ., 30, 3599–3609, https://doi.org/10.1016/1352-2310(96)00069-6, 1996.

Feng, Y., Ning, M., Lei, Y., Sun, Y., Liu, W., and Wang, J.: Defending blue sky in China: Effectiveness of the "Air Pollution Prevention and Control Action Plan" on air quality improvements from 2013 to 2017, J. Environ. Manage., 252, 109603, https://doi.org/10.1016/j.jenvman.2019.109603, 2019.

Finlayson-Pitts, B. J. and Pitts, J. N.: CHAPTER 4 – Photochemistry of Important Atmospheric Species, in: Chemistry of the Upper and Lower Atmosphere, edited by: Finlayson-Pitts, B. J. and Pitts, J. N., Academic Press, San Diego, 86–129, https://doi.org/10.1016/B978-012257060-5/50006-X, 2000.

Finlayson-Pitts, B. J., Wingen, L. M., Sumner, A. L., Syomin, D., and Ramazan, K. A.: The heterogeneous hydrolysis of NO_2 in laboratory systems and in outdoor and indoor atmospheres: An integrated mechanism, Phys. Chem. Chem. Phys., 5, 223–242, https://doi.org/10.1039/B208564J, 2003.

Gall, E. T., Griffin, R. J., Steiner, A. L., Dibb, J., Scheuer, E., Gong, L., Rutter, A. P., Cevik, B. K., Kim, S., Lefer, B., and Flynn, J.: Evaluation of nitrous acid sources and sinks in urban outflow, Atmos. Environ., 127, 272–282, https://doi.org/10.1016/j.atmosenv.2015.12.044, 2016.

Ge, S., Wang, G., Zhang, S., Li, D., Xie, Y., Wu, C., Yuan, Q., Chen, J., and Zhang, H.: Abundant NH_3 in China Enhances Atmospheric HONO Production by Promoting the Heterogeneous Reaction of SO_2 with NO_2, Environ. Sci. Technol., 53, 14339–14347, https://doi.org/10.1021/acs.est.9b04196, 2019.

Gen, M., Zhang, R., and Chan, C. K.: Nitrite/Nitrous Acid Generation from the Reaction of Nitrate and Fe(II) Promoted by Photolysis of Iron–Organic Complexes, Environ. Sci. Technol., 55, 15715–15723, https://doi.org/10.1021/acs.est.1c05641, 2021.

Gerecke, A., Thielmann, A., Gutzwiller, L., and Rossi, M. J.: The chemical kinetics of HONO formation resulting from heterogeneous interaction of NO_2 with flame soot, Geophys. Res. Lett., 25, 2453–2456, https://doi.org/10.1029/98GL01796, 1998.

Gu, R., Shen, H., Xue, L., Wang, T., Gao, J., Li, H., Liang, Y., Xia, M., Yu, C., Liu, Y., and Wang, W.: Investigating the sources of atmospheric nitrous acid (HONO) in the megacity of Beijing, China, Sci. Total Environ., 812, 152270, https://doi.org/10.1016/j.scitotenv.2021.152270, 2021.

Gutzwiller, L., Arens, F., Baltensperger, U., Gäggeler, H. W., and Ammann, M.: Significance of Semivolatile Diesel Exhaust Organics for Secondary HONO Formation, Environ. Sci. Technol., 36, 677–682, https://doi.org/10.1021/es015673b, 2002.

Han, C., Liu, Y., and He, H.: Heterogeneous reaction of NO_2 with soot at different relative humidity, Environ. Sci. Pollut. R., 24, 21248–21255, https://doi.org/10.1007/s11356-017-9766-y, 2017a.

Han, C., Yang, W., Yang, H., and Xue, X.: Enhanced photochemical conversion of NO_2 to HONO on humic acids in the presence of benzophenone, Environ. Pollut., 231, 979–986, https://doi.org/10.1016/j.envpol.2017.08.107, 2017b.

Hao, Q., Jiang, N., Zhang, R., Yang, L., and Li, S.: Characteristics, sources, and reactions of nitrous acid during winter at an urban site in the Central Plains Economic Region in China, Atmos. Chem. Phys., 20, 7087–7102, https://doi.org/10.5194/acp-20-7087-2020, 2020.

Harrison, R. M. and Kitto, A.-M. N.: Evidence for a surface source of atmospheric nitrous acid, Atmos. Environ., 28, 1089–1094, https://doi.org/10.1016/1352-2310(94)90286-0, 1994.

Heard, D. E., Carpenter, L. J., Creasey, D. J., Hopkins, J. R., Lee, J. D., Lewis, A. C., Pilling, M. J., Seakins, P. W., Carslaw, N., and Emmerson, K. M.: High levels of the hydroxyl radical in the winter urban troposphere, Geophys. Res. Lett., 31, L18112, https://doi.org/10.1029/2004GL020544, 2004.

Heland, J., Kleffmann, J., Kurtenbach, R., and Wiesen, P.: A New Instrument To Measure Gaseous Nitrous Acid (HONO) in the Atmosphere, Environ. Sci. Technol., 35, 3207–3212, https://doi.org/10.1021/es000303t, 2001.

Hendrick, F., Müller, J.-F., Clémer, K., Wang, P., De Mazière, M., Fayt, C., Gielen, C., Hermans, C., Ma, J. Z., Pinardi, G., Stavrakou, T., Vlemmix, T., and Van Roozendael, M.: Four years of ground-based MAX-DOAS observations of HONO and NO2 in the Beijing area, Atmos. Chem. Phys., 14, 765–781, https://doi.org/10.5194/acp-14-765-2014, 2014.

Hofzumahaus, A., Rohrer, F., Lu, K., Bohn, B., Brauers, T., Chang, C.-C., Fuchs, H., Holland, F., Kita, K., Kondo, Y., Li, X., Lou, S., Shao, M., Zeng, L., Wahner, A., and Zhang, Y.: Amplified Trace Gas Removal in the Troposphere, Science, 324, 1702–1704, https://doi.org/10.1126/science.1164566, 2009.

Hou, S., Tong, S., Ge, M., and An, J.: Comparison of atmospheric nitrous acid during severe haze and clean periods in Beijing, China, Atmos. Environ., 124, 199–206, https://doi.org/10.1016/j.atmosenv.2015.06.023, 2016.

Hu, M., Zhou, F., Shao, K., Zhang, Y., Tang, X., and Slanina, J.: Diurnal variations of aerosol chemical compositions and related gaseous pollutants in Beijing and Guangzhou, J. Environ. Sci. Heal. A, 37, 479–488, https://doi.org/10.1081/ESE-120003229, 2002.

Huang, R. J., Yang, L., Cao, J., Wang, Q., Tie, X., Ho, K. F., Shen, Z., Zhang, R., Li, G., Zhu, C., Zhang, N., Dai, W., Zhou, J., Liu, S., Chen, Y., Chen, J., and O'Dowd, C. D.: Concentration and sources of atmospheric nitrous acid (HONO) at an urban site in Western China, Sci. Total Environ., 593–594, 165–172, https://doi.org/10.1016/j.scitotenv.2017.02.166, 2017.

Huang, Z., Zhong, Z., Sha, Q., Xu, Y., Zhang, Z., Wu, L., Wang, Y., Zhang, L., Cui, X., Tang, M., Shi, B., Zheng, C., Li, Z., Hu, M., Bi, L., Zheng, J., and Yan, M.: An updated model-ready emission inventory for Guangdong Province by incorporating big data and mapping onto multiple chemical mechanisms, Sci. Total Environ., 769, 144535, https://doi.org/10.1016/j.scitotenv.2020.144535, 2021.

Jia, C., Tong, S., Zhang, W., Zhang, X., Li, W., Wang, Z., Wang, L., Liu, Z., Hu, B., Zhao, P., and Ge, M.: Pollution characteristics and potential sources of nitrous acid (HONO) in early autumn 2018 of Beijing, Sci. Total Environ., 735, 139317, https://doi.org/10.1016/j.scitotenv.2020.139317, 2020.

Jiang, Y., Xue, L., Gu, R., Jia, M., Zhang, Y., Wen, L., Zheng, P., Chen, T., Li, H., Shan, Y., Zhao, Y., Guo, Z., Bi, Y., Liu, H., Ding, A., Zhang, Q., and Wang, W.: Sources of nitrous acid (HONO) in the upper boundary layer and lower free troposphere of the North China Plain: insights from the Mount Tai Observatory, Atmos. Chem. Phys., 20, 12115–12131, https://doi.org/10.5194/acp-20-12115-2020, 2020.

Kaiser, E. W. and Wu, C. H.: A kinetic study of the gas phase formation and decomposition reactions of nitrous acid, J. Phys. Chem., 81, 1701–1706, https://doi.org/10.1021/j100533a001, 1977.

Kalberer, M., Ammann, M., Arens, F., Gäggeler, H. W., and Baltensperger, U.: Heterogeneous formation of nitrous acid (HONO) on soot aerosol particles, J. Geophys. Res.-Atmos., 104, 13825–13832, https://doi.org/10.1029/1999JD900141, 1999.

Kinugawa, T., Enami, S., Yabushita, A., Kawasaki, M., Hoffmann, M. R., and Colussi, A. J.: Conversion of gaseous nitrogen dioxide to nitrate and nitrite on aqueous surfactants, Phys. Chem. Chem. Phys., 13, 5144–5149, https://doi.org/10.1039/C0CP01497D, 2011.

Kirchstetter, T. W., Harley, R. A., and Littlejohn, D.: Measurement of Nitrous Acid in Motor Vehicle Exhaust, Environ. Sci. Technol., 30, 2843–2849, https://doi.org/10.1021/es960135y, 1996.

Kleffmann, J., Kurtenbach, R., Lörzer, J., Wiesen, P., Kalthoff, N., Vogel, B., and Vogel, H.: Measured and simulated vertical profiles of nitrous acid—Part I: Field measurements, Atmos. Environ., 37, 2949–2955, https://doi.org/10.1016/S1352-2310(03)00242-5, 2003.

Kleffmann, J., Gavriloaiei, T., Hofzumahaus, A., Holland, F., Koppmann, R., Rupp, L., Schlosser, E., Siese, M., and Wahner, A.: Daytime formation of nitrous acid: A major source of OH radicals in a forest, Geophys. Res. Lett., 32, L05818, https://doi.org/10.1029/2005GL022524, 2005.

Kleffmann, J., Lörzer, J. C., Wiesen, P., Kern, C., Trick, S., Volkamer, R., Rodenas, M., and Wirtz, K.: Intercomparison of the DOAS and LOPAP techniques for the detection of nitrous acid (HONO), Atmos. Environ., 40, 3640–3652, https://doi.org/10.1016/j.atmosenv.2006.03.027, 2006.

Kramer, L. J., Crilley, L. R., Adams, T. J., Ball, S. M., Pope, F. D., and Bloss, W. J.: Nitrous acid (HONO) emissions under real-world driving conditions from vehicles in a UK road tunnel, Atmos. Chem. Phys., 20, 5231–5248, https://doi.org/10.5194/acp-20-5231-2020, 2020.

Kurtenbach, R., Becker, K. H., Gomes, J. A. G., Kleffmann, J., Lörzer, J. C., Spittler, M., Wiesen, P., Ackermann, R., Geyer, A., and Platt, U.: Investigations of emissions and heterogeneous formation of HONO in a road traffic tunnel, Atmos. Environ., 35, 3385–3394, https://doi.org/10.1016/S1352-2310(01)00138-8, 2001.

Lammel, G. and Cape, J. N.: Nitrous acid and nitrite in the atmosphere, Chem. Soc. Rev., 25, 361–369, https://doi.org/10.1039/CS9962500361, 1996.

Lee, J. D., Whalley, L. K., Heard, D. E., Stone, D., Dunmore, R. E., Hamilton, J. F., Young, D. E., Allan, J. D., Laufs, S., and Kleffmann, J.: Detailed budget analysis of HONO in central London reveals a missing daytime source, Atmos. Chem. Phys., 16, 2747–2764, https://doi.org/10.5194/acp-16-2747-2016, 2016.

Lelieveld, J., Gromov, S., Pozzer, A., and Taraborrelli, D.: Global tropospheric hydroxyl distribution, budget and reactivity, Atmos. Chem. Phys., 16, 12477–12493, https://doi.org/10.5194/acp-16-12477-2016, 2016.

Li, D., Xue, L., Wen, L., Wang, X., Chen, T., Mellouki, A., Chen, J., and Wang, W.: Characteristics and sources of nitrous acid in an urban atmosphere of northern China: Results from 1-yr continuous observations, Atmos. Environ., 182, 296–306, https://doi.org/10.1016/j.atmosenv.2018.03.033, 2018.

Li, J., Lu, K., Lv, W., Li, J., Zhong, L., Ou, Y., Chen, D., Huang, X., and Zhang, Y.: Fast increasing of surface ozone concentrations in Pearl River Delta characterized by a regional air quality monitoring network during 2006–2011, J. Environ. Sci., 26, 23–36, https://doi.org/10.1016/S1001-0742(13)60377-0, 2014.

Li, L., Duan, Z., Li, H., Zhu, C., Henkelman, G., Francisco, J. S., and Zeng, X. C.: Formation of HONO from the NH_3 promoted hydrolysis of NO_2 dimers in the atmosphere, P. Natl. Acad. Sci., 115, 7236–7241, https://doi.org/10.1073/pnas.1807719115, 2018.

Li, W., Tong, S., Cao, J., Su, H., Zhang, W., Wang, L., Jia, C., Zhang, X., Wang, Z., Chen, M., and Ge, M.: Comparative observation of atmospheric nitrous acid (HONO) in Xi'an and Xianyang located in the GuanZhong basin of western China, Environ. Pollut., 289, 117679, https://doi.org/10.1016/j.envpol.2021.117679, 2021.

Li, X., Brauers, T., Häseler, R., Bohn, B., Fuchs, H., Hofzumahaus, A., Holland, F., Lou, S., Lu, K. D., Rohrer, F., Hu, M., Zeng, L. M., Zhang, Y. H., Garland, R. M., Su, H., Nowak, A., Wiedensohler, A., Takegawa, N., Shao, M., and Wahner, A.: Exploring the atmospheric chemistry of nitrous acid (HONO) at a rural site in Southern China, Atmos. Chem. Phys., 12, 1497–1513, https://doi.org/10.5194/acp-12-1497-2012, 2012.

Li, X., Rohrer, F., Hofzumahaus, A., Brauers, T., Häseler, R., Bohn, B., Broch, S., Fuchs, H., Gomm, S., Holland, F., Jäger, J., Kaiser, J., Keutsch, F. N., Lohse, I., Lu, K., Tillmann, R., Wegener, R., Wolfe, G. M., Mentel, T. F., Kiendler-Scharr, A., and Wahner, A.: Missing Gas-Phase Source of HONO Inferred from Zeppelin Measurements in the Troposphere, Science, 344, 292–296, https://doi.org/10.1126/science.1248999, 2014.

Li, Y., An, J., Min, M., Zhang, W., Wang, F., and Xie, P.: Impacts of HONO sources on the air quality in Beijing, Tianjin and Hebei Province of China, Atmos. Environ., 45, 4735–4744, https://doi.org/10.1016/j.atmosenv.2011.04.086, 2011.

Liao, B., Huang, J., Wang, C., Weng, J., Li, L., Cai, H., and D, W.: Comparative analysis on the boundary layer features of haze processes and cleaning process in Guangzhou, China Environmental Science, 38, 4432–4443, http://www.zghjkx.com.cn/CN/Y2018/V38/I12/4432 (last access: 10 June 2022), 2018.

Liao, W., Wu, L., Zhou, S., Wang, X., and Chen, D.: Impact of Synoptic Weather Types on Ground-Level Ozone Concentrations in Guangzhou, China, Asia-Pac. J. Atmos. Sci., https://doi.org/10.1007/s13143-020-00186-2, 2020.

Lin, Y.-C., Cheng, M.-T., Ting, W.-Y., and Yeh, C.-R.: Characteristics of gaseous HNO_2, HNO_3, NH_3 and particulate ammonium nitrate in an urban city of Central Taiwan, Atmos. Environ., 40, 4725–4733, https://doi.org/10.1016/j.atmosenv.2006.04.037, 2006.

Liu, J., Liu, Z., Ma, Z., Yang, S., Yao, D., Zhao, S., Hu, B., Tang, G., Sun, J., Cheng, M., Xu, Z., and Wang, Y.: Detailed budget analysis of HONO in Beijing, China: Implication on atmosphere oxidation capacity in polluted megacity, Atmos. Environ., 244, 117957, https://doi.org/10.1016/j.atmosenv.2020.117957, 2021.

Liu, Y.: Observations and parameterized modelling of ambient nitrous acid (HONO) in the megacity areas of the eastern China, PhD thesis, College of Environmental Sciences and Engineering, Peking University, China, 2017.

Liu, Y., Lu, K., Ma, Y., Yang, X., Zhang, W., Wu, Y., Peng, J., Shuai, S., Hu, M., and Zhang, Y.: Direct emission of nitrous acid (HONO) from gasoline cars in China determined by vehicle chassis dynamometer experiments, Atmos. Environ., 169, 89–96, https://doi.org/10.1016/j.atmosenv.2017.07.019, 2017.

Liu, Y., Lu, K., Li, X., Dong, H., Tan, Z., Wang, H., Zou, Q., Wu, Y., Zeng, L., Hu, M., Min, K. E., Kecorius, S., Wiedensohler, A., and Zhang, Y.: A Comprehensive Model Test of the HONO Sources Constrained to Field Measurements at Rural North China Plain, Environ. Sci. Technol., 53, 3517–3525, https://doi.org/10.1021/acs.est.8b06367, 2019a.

Liu, Y., Nie, W., Xu, Z., Wang, T., Wang, R., Li, Y., Wang, L., Chi, X., and Ding, A.: Semi-quantitative understanding of source contribution to nitrous acid (HONO) based on 1 year of continuous observation at the SORPES station in eastern China, Atmos. Chem. Phys., 19, 13289–13308, https://doi.org/10.5194/acp-19-13289-2019, 2019b.

Liu, Y., Ni, S., Jiang, T., Xing, S., Zhang, Y., Bao, X., Feng, Z., Fan, X., Zhang, L., and Feng, H.: Influence of Chinese New Year overlapping COVID-19 lockdown on HONO sources in Shijiazhuang, Sci. Total Environ., 745, 141025, https://doi.org/10.1016/j.scitotenv.2020.141025, 2020a.

Liu, Y., Zhang, Y., Lian, C., Yan, C., Feng, Z., Zheng, F., Fan, X., Chen, Y., Wang, W., Chu, B., Wang, Y., Cai, J., Du, W., Daellenbach, K. R., Kangasluoma, J., Bianchi, F., Kujansuu, J., Petäjä, T., Wang, X., Hu, B., Wang, Y., Ge, M., He, H., and Kulmala, M.: The promotion effect of nitrous acid on aerosol formation in wintertime in Beijing: the possible contribution of traffic-related emissions, Atmos. Chem. Phys., 20, 13023–13040, https://doi.org/10.5194/acp-20-13023-2020, 2020b.

Liu, Z., Wang, Y., Costabile, F., Amoroso, A., Zhao, C., Huey, L. G., Stickel, R., Liao, J., and Zhu, T.: Evidence of aerosols as a media for rapid daytime HONO production over China, Environ. Sci. Technol., 48, 14386–14391, https://doi.org/10.1021/es504163z, 2014.

Lou, S., Holland, F., Rohrer, F., Lu, K., Bohn, B., Brauers, T., Chang, C. C., Fuchs, H., Häseler, R., Kita, K., Kondo, Y., Li, X., Shao, M., Zeng, L., Wahner, A., Zhang, Y., Wang, W., and Hofzumahaus, A.: Atmospheric OH reactivities in the Pearl River Delta – China in summer 2006: measurement and model results, Atmos. Chem. Phys., 10, 11243–11260, https://doi.org/10.5194/acp-10-11243-2010, 2010.

Lu, K. D., Rohrer, F., Holland, F., Fuchs, H., Bohn, B., Brauers, T., Chang, C. C., Häseler, R., Hu, M., Kita, K., Kondo, Y., Li, X., Lou, S. R., Nehr, S., Shao, M., Zeng, L. M., Wahner, A., Zhang, Y. H., and Hofzumahaus, A.: Observation and modelling of OH and HO_2 concentrations in the Pearl River Delta 2006: a missing OH source in a VOC rich atmosphere, Atmos. Chem. Phys., 12, 1541–1569, https://doi.org/10.5194/acp-12-1541-2012, 2012.

Lu, K. D., Hofzumahaus, A., Holland, F., Bohn, B., Brauers, T., Fuchs, H., Hu, M., Häseler, R., Kita, K., Kondo, Y., Li, X., Lou, S. R., Oebel, A., Shao, M., Zeng, L. M., Wahner, A., Zhu, T., Zhang, Y. H., and Rohrer, F.: Missing OH source in a suburban environment near Beijing: observed and modelled OH and HO_2 concentrations in summer 2006, Atmos. Chem. Phys., 13, 1057–1080, https://doi.org/10.5194/acp-13-1057-2013, 2013.

Lu, K. D., Rohrer, F., Holland, F., Fuchs, H., Brauers, T., Oebel, A., Dlugi, R., Hu, M., Li, X., Lou, S. R., Shao, M., Zhu, T., Wahner, A., Zhang, Y. H., and Hofzumahaus, A.: Nighttime observation and chemistry of HO_x in the Pearl River Delta and Beijing in summer 2006, Atmos. Chem. Phys., 14, 4979–4999, https://doi.org/10.5194/acp-14-4979-2014, 2014.

Lu, X., Hong, J., Zhang, L., Cooper, O. R., Schultz, M. G., Xu, X., Wang, T., Gao, M., Zhao, Y., and Zhang, Y.: Severe Surface Ozone Pollution in China: A Global Perspective, Environ. Sci. Tech. Let., 5, 487–494, https://doi.org/10.1021/acs.estlett.8b00366, 2018.

Mebel, A. M., Lin, M. C., and Melius, C. F.: Rate Constant of the $HONO + HONO \rightarrow H_2O + NO + NO_2$ Reaction from ab Initio MO and TST Calculations, J. Phys. Chem. A, 102, 1803–1807, https://doi.org/10.1021/jp973449w, 1998.

Meng, F., Qin, M., Tang, K., Duan, J., Fang, W., Liang, S., Ye, K., Xie, P., Sun, Y., Xie, C., Ye, C., Fu, P., Liu, J., and Liu, W.: High-resolution vertical distribution and sources of HONO and NO_2 in the nocturnal boundary layer in urban Beijing, China, Atmos. Chem. Phys., 20, 5071–5092, https://doi.org/10.5194/acp-20-5071-2020, 2020.

Meusel, H., Kuhn, U., Reiffs, A., Mallik, C., Harder, H., Martinez, M., Schuladen, J., Bohn, B., Parchatka, U., Crowley, J. N., Fischer, H., Tomsche, L., Novelli, A., Hoffmann, T., Janssen, R. H. H., Hartogensis, O., Pikridas, M., Vrekoussis, M., Bourtsoukidis, E., Weber, B., Lelieveld, J., Williams, J., Pöschl, U., Cheng, Y., and Su, H.: Daytime formation of nitrous acid at a coastal remote site in Cyprus indicating a common ground source of atmospheric HONO and NO, Atmos. Chem. Phys., 16, 14475–14493, https://doi.org/10.5194/acp-16-14475-2016, 2016.

Michoud, V., Kukui, A., Camredon, M., Colomb, A., Borbon, A., Miet, K., Aumont, B., Beekmann, M., Durand-Jolibois, R., Perrier, S., Zapf, P., Siour, G., Ait-Helal, W., Locoge, N., Sauvage, S., Afif, C., Gros, V., Furger, M., Ancellet, G., and Doussin, J. F.: Radical budget analysis in a suburban European site during the MEGAPOLI summer field campaign, Atmos. Chem. Phys., 12, 11951–11974, https://doi.org/10.5194/acp-12-11951-2012, 2012.

Michoud, V., Colomb, A., Borbon, A., Miet, K., Beekmann, M., Camredon, M., Aumont, B., Perrier, S., Zapf, P., Siour, G., Ait-Helal, W., Afif, C., Kukui, A., Furger, M., Dupont, J. C., Haeffelin, M., and Doussin, J. F.: Study of the unknown HONO daytime source at a European suburban site during the MEGAPOLI summer and winter field campaigns, Atmos. Chem. Phys., 14, 2805–2822, https://doi.org/10.5194/acp-14-2805-2014, 2014.

Monge, M. E., D'Anna, B., Mazri, L., Giroir-Fendler, A., Ammann, M., Donaldson, D. J., and George, C.: Light changes the atmospheric reactivity of soot, P. Natl. Acad. Sci., 107, 6605–6609, https://doi.org/10.1073/pnas.0908341107, 2010.

Nakashima, Y. and Kajii, Y.: Determination of nitrous acid emission factors from a gasoline vehicle using a chassis dynamometer combined with incoherent broadband cavity-enhanced absorption spectroscopy, Sci. Total Environ., 575, 287–293, https://doi.org/10.1016/j.scitotenv.2016.10.050, 2017.

Oswald, R., Behrendt, T., Ermel, M., Wu, D., Su, H., Cheng, Y., Breuninger, C., Moravek, A., Mougin, E., Delon, C., Loubet, B., Pommerening-Röser, A., Sörgel, M., Pöschl, U., Hoffmann, T., Andreae, M. O., Meixner, F. X., and Trebs, I.: HONO Emissions from Soil Bacteria as a Major Source of Atmospheric Reactive Nitrogen, Science, 341, 1233–1235, https://doi.org/10.1126/science.1242266, 2013.

Perner, D. and Platt, U.: Detection of nitrous acid in the atmosphere by differential optical absorption, Geophys. Res. Lett., 6, 917–920, https://doi.org/10.1029/GL006i012p00917, 1979.

Pitts, J. N., Biermann, H. W., Winer, A. M., and Tuazon, E. C.: Spectroscopic identification and measurement of gaseous nitrous acid in dilute auto exhaust, Atmos. Environ., 18, 847–854, https://doi.org/10.1016/0004-6981(84)90270-1, 1984.

Pusede, S. E., VandenBoer, T. C., Murphy, J. G., Markovic, M. Z., Young, C. J., Veres, P. R., Roberts, J. M., Washenfelder, R. A., Brown, S. S., Ren, X., Tsai, C., Stutz, J., Brune, W. H., Browne, E. C., Wooldridge, P. J., Graham, A. R., Weber, R., Goldstein, A. H., Dusanter, S., Griffith, S. M., Stevens, P. S., Lefer, B. L., and Cohen, R. C.: An Atmospheric Constraint on the NO_2 Dependence of Daytime Near-Surface Nitrous Acid (HONO), Environ. Sci. Technol., 49, 12774–12781, https://doi.org/10.1021/acs.est.5b02511, 2015.

Qin, M., Xie, P., Su, H., Gu, J., Peng, F., Li, S., Zeng, L., Liu, J., Liu, W., and Zhang, Y.: An observational study of the HONO–NO_2 coupling at an urban site in Guangzhou City, South China, Atmos. Environ., 43, 5731–5742, https://doi.org/10.1016/j.atmosenv.2009.08.017, 2009.

Rappenglück, B., Lubertino, G., Alvarez, S., Golovko, J., Czader, B., and Ackermann, L.: Radical precursors and re-

lated species from traffic as observed and modeled at an urban highway junction, J. Air Waste Manage., 63, 1270–1286, https://doi.org/10.1080/10962247.2013.822438, 2013.

Reisinger, A. R.: Observations of HNO_2 in the polluted winter atmosphere: possible heterogeneous production on aerosols, Atmos. Environ., 34, 3865–3874, https://doi.org/10.1016/S1352-2310(00)00179-5, 2000.

Rohrer, F. and Berresheim, H.: Strong correlation between levels of tropospheric hydroxyl radicals and solar ultraviolet radiation, Nature, 442, 184–187, https://doi.org/10.1038/nature04924, 2006.

Romanias, M. N., El Zein, A., and Bedjanian, Y.: Reactive uptake of HONO on aluminium oxide surface, J. Photoch. Photobio. A, 250, 50–57, https://doi.org/10.1016/j.jphotochem.2012.09.018, 2012.

Saliba, N. A., Yang, H., and Finlayson-Pitts, B. J.: Reaction of Gaseous Nitric Oxide with Nitric Acid on Silica Surfaces in the Presence of Water at Room Temperature, J. Phys. Chem. A, 105, 10339–10346, https://doi.org/10.1021/jp012330r, 2001.

Shao, M., Ren, X., Wang, H., Zeng, L., Zhang, Y., and Tang, X.: Quantitative relationship between production and removal of OH and HO_2 radicals in urban atmosphere, Chinese Sci. Bull., 49, 2253–2258, https://link.springer.com/article/10.1360/04wb0006 (last access: 30 June 2022), 2004.

Shi, X., Ge, Y., Zheng, J., Ma, Y., Ren, X., and Zhang, Y.: Budget of nitrous acid and its impacts on atmospheric oxidative capacity at an urban site in the central Yangtze River Delta region of China, Atmos. Environ., 238, 117725, https://doi.org/10.1016/j.atmosenv.2020.117725, 2020.

Slater, E. J., Whalley, L. K., Woodward-Massey, R., Ye, C., Lee, J. D., Squires, F., Hopkins, J. R., Dunmore, R. E., Shaw, M., Hamilton, J. F., Lewis, A. C., Crilley, L. R., Kramer, L., Bloss, W., Vu, T., Sun, Y., Xu, W., Yue, S., Ren, L., Acton, W. J. F., Hewitt, C. N., Wang, X., Fu, P., and Heard, D. E.: Elevated levels of OH observed in haze events during wintertime in central Beijing, Atmos. Chem. Phys., 20, 14847–14871, https://doi.org/10.5194/acp-20-14847-2020, 2020.

Song, L., Deng, T., and Wu, D.: Study on planetary boundary layer height in a typical haze period and different weather types over Guangzhou, Acta Scientiae Circumstantiae, 39, 1381–1391, https://doi.org/10.13671/j.hjkxxb.2019.0080, 2019.

Sörgel, M., Regelin, E., Bozem, H., Diesch, J.-M., Drewnick, F., Fischer, H., Harder, H., Held, A., Hosaynali-Beygi, Z., Martinez, M., and Zetzsch, C.: Quantification of the unknown HONO daytime source and its relation to NO_2, Atmos. Chem. Phys., 11, 10433–10447, https://doi.org/10.5194/acp-11-10433-2011, 2011a.

Sörgel, M., Trebs, I., Serafimovich, A., Moravek, A., Held, A., and Zetzsch, C.: Simultaneous HONO measurements in and above a forest canopy: influence of turbulent exchange on mixing ratio differences, Atmos. Chem. Phys., 11, 841–855, https://doi.org/10.5194/acp-11-841-2011, 2011b.

Stemmler, K., Ammann, M., Donders, C., Kleffmann, J., and George, C.: Photosensitized reduction of nitrogen dioxide on humic acid as a source of nitrous acid, Nature, 440, 195–198, https://doi.org/10.1038/nature04603, 2006.

Stutz, J., Kim, E. S., Platt, U., Bruno, P., Perrino, C., and Febo, A.: UV-visible absorption cross sections of nitrous acid, J. Geophys. Res.-Atmos., 105, 14585–14592, https://doi.org/10.1029/2000JD900003, 2000.

Stutz, J., Alicke, B., and Neftel, A.: Nitrous acid formation in the urban atmosphere: Gradient measurements of NO_2 and HONO over grass in Milan, Italy, J. Geophys. Res.-Atmos., 107, 8192, https://doi.org/10.1029/2001JD000390, 2002.

Stutz, J., Alicke, B., Ackermann, R., Geyer, A., Wang, S., White, A. B., Williams, E. J., Spicer, C. W., and Fast, J. D.: Relative humidity dependence of HONO chemistry in urban areas, J. Geophys. Res.-Atmos., 109, D03307, https://doi.org/10.1029/2003JD004135, 2004.

Su, H.: HONO: a study to its sources and impacts from field measurements at the sub-urban areas of PRD region, PhD thesis, College of Environmental Sciences and Engineering, Peking University, China, http://cdmd.cnki.com.cn/Article/CDMD-10001-2008082105.htm (last access: 10 June 2022), 2008.

Su, H., Cheng, Y. F., Cheng, P., Zhang, Y. H., Dong, S., Zeng, L. M., Wang, X., Slanina, J., Shao, M., and Wiedensohler, A.: Observation of nighttime nitrous acid (HONO) formation at a non-urban site during PRIDE-PRD2004 in China, Atmos. Environ., 42, 6219–6232, https://doi.org/10.1016/j.atmosenv.2008.04.006, 2008a.

Su, H., Cheng, Y. F., Shao, M., Gao, D. F., Yu, Z. Y., Zeng, L. M., Slanina, J., Zhang, Y. H., and Wiedensohler, A.: Nitrous acid (HONO) and its daytime sources at a rural site during the 2004 PRIDE-PRD experiment in China, J. Geophys. Res., 113, D14312, https://doi.org/10.1029/2007JD009060, 2008b.

Su, H., Cheng, Y., Oswald, R., Behrendt, T., Trebs, I., Meixner, F. X., Andreae, M. O., Cheng, P., Zhang, Y., and Pöschl, U.: Soil Nitrite as a Source of Atmospheric HONO and OH Radicals, Science, 333, 1616–1618, https://doi.org/10.1126/science.1207687, 2011.

Tan, Z., Fuchs, H., Lu, K., Hofzumahaus, A., Bohn, B., Broch, S., Dong, H., Gomm, S., Häseler, R., He, L., Holland, F., Li, X., Liu, Y., Lu, S., Rohrer, F., Shao, M., Wang, B., Wang, M., Wu, Y., Zeng, L., Zhang, Y., Wahner, A., and Zhang, Y.: Radical chemistry at a rural site (Wangdu) in the North China Plain: observation and model calculations of OH, HO_2 and RO_2 radicals, Atmos. Chem. Phys., 17, 663–690, https://doi.org/10.5194/acp-17-663-2017, 2017.

Tan, Z., Rohrer, F., Lu, K., Ma, X., Bohn, B., Broch, S., Dong, H., Fuchs, H., Gkatzelis, G. I., Hofzumahaus, A., Holland, F., Li, X., Liu, Y., Liu, Y., Novelli, A., Shao, M., Wang, H., Wu, Y., Zeng, L., Hu, M., Kiendler-Scharr, A., Wahner, A., and Zhang, Y.: Wintertime photochemistry in Beijing: observations of RO_x radical concentrations in the North China Plain during the BEST-ONE campaign, Atmos. Chem. Phys., 18, 12391–12411, https://doi.org/10.5194/acp-18-12391-2018, 2018.

Tan, Z., Lu, K., Hofzumahaus, A., Fuchs, H., Bohn, B., Holland, F., Liu, Y., Rohrer, F., Shao, M., Sun, K., Wu, Y., Zeng, L., Zhang, Y., Zou, Q., Kiendler-Scharr, A., Wahner, A., and Zhang, Y.: Experimental budgets of OH, HO_2, and RO_2 radicals and implications for ozone formation in the Pearl River Delta in China 2014, Atmos. Chem. Phys., 19, 7129–7150, https://doi.org/10.5194/acp-19-7129-2019, 2019.

Tang, X. Y.: The characteristics of urban air pollution in China, in Urbanization, energy, and air pollution in China: The challenges ahead, Proceedings of A Symposium, Na-

tional Academies Press, 47–54, ISBN 978-0-309-09323-1 https://doi.org/10.17226/11192, 2004.

Tian, Z., Yang, W., Yu, X., Zhang, M., Zhang, H., Cheng, D., Cheng, P., and Wang, B.: HONO pollution characteristics and nighttime sources during autumn in Guangzhou, China Environmental Science, 39, 2000–2009, https://doi.org/10.13227/j.hjkx.201709269, 2018.

Tong, S., Hou, S., Zhang, Y., Chu, B., Liu, Y., He, H., Zhao, P., and Ge, M.: Comparisons of measured nitrous acid (HONO) concentrations in a pollution period at urban and suburban Beijing, in autumn of 2014, Science China Chemistry, 58, 1393–1402, https://doi.org/10.1007/s11426-015-5454-2, 2015.

Tong, S., Hou, S., Zhang, Y., Chu, B., Liu, Y., He, H., Zhao, P., and Ge, M.: Exploring the nitrous acid (HONO) formation mechanism in winter Beijing: direct emissions and heterogeneous production in urban and suburban areas, Faraday Discuss., 189, 213–230, https://doi.org/10.1039/C5FD00163C, 2016.

Trinh, H. T., Imanishi, K., Morikawa, T., Hagino, H., and Takenaka, N.: Gaseous nitrous acid (HONO) and nitrogen oxides (NO_x) emission from gasoline and diesel vehicles under real-world driving test cycles, J. Air Waste Manage., 67, 412–420, https://doi.org/10.1080/10962247.2016.1240726, 2017.

Tsai, C., Spolaor, M., Colosimo, S. F., Pikelnaya, O., Cheung, R., Williams, E., Gilman, J. B., Lerner, B. M., Zamora, R. J., Warneke, C., Roberts, J. M., Ahmadov, R., de Gouw, J., Bates, T., Quinn, P. K., and Stutz, J.: Nitrous acid formation in a snow-free wintertime polluted rural area, Atmos. Chem. Phys., 18, 1977–1996, https://doi.org/10.5194/acp-18-1977-2018, 2018.

VandenBoer, T. C., Brown, S. S., Murphy, J. G., Keene, W. C., Young, C. J., Pszenny, A. A. P., Kim, S., Warneke, C., de Gouw, J. A., Maben, J. R., Wagner, N. L., Riedel, T. P., Thornton, J. A., Wolfe, D. E., Dubé, W. P., Öztürk, F., Brock, C. A., Grossberg, N., Lefer, B., Lerner, B., Middlebrook, A. M., and Roberts, J. M.: Understanding the role of the ground surface in HONO vertical structure: High resolution vertical profiles during NACHTT-11, J. Geophys. Res.-Atmos., 118, 10155–110171, https://doi.org/10.1002/jgrd.50721, 2013.

Villena, G., Kleffmann, J., Kurtenbach, R., Wiesen, P., Lissi, E., Rubio, M. A., Croxatto, G., and Rappenglück, B.: Vertical gradients of HONO, NO_x and O_3 in Santiago de Chile, Atmos. Environ., 45, 3867–3873, https://doi.org/10.1016/j.atmosenv.2011.01.073, 2011.

Vogel, B., Vogel, H., Kleffmann, J., and Kurtenbach, R.: Measured and simulated vertical profiles of nitrous acid – Part II. Model simulations and indications for a photolytic source, Atmos. Environ., 37, 2957–2966, https://doi.org/10.1016/S1352-2310(03)00243-7, 2003.

Voogt, J. A. and Oke, T. R.: Complete Urban Surface Temperatures, J. Appl. Meteorol., 36, 1117–1132, https://doi.org/10.1175/1520-0450(1997)036<1117:CUST>2.0.CO;2, 1997.

Wall, K. J. and Harris, G. W.: Uptake of nitrogen dioxide (NO_2) on acidic aqueous humic acid (HA) solutions as a missing daytime nitrous acid (HONO) surface source, J. Atmos. Chem., 74, 283–321, https://doi.org/10.1007/s10874-016-9342-8, 2017.

Wang, G., Zhang, R., Gomez, M. E., Yang, L., Levy Zamora, M., Hu, M., Lin, Y., Peng, J., Guo, S., Meng, J., Li, J., Cheng, C., Hu, T., Ren, Y., Wang, Y., Gao, J., Cao, J., An, Z., Zhou, W., Li, G., Wang, J., Tian, P., Marrero-Ortiz, W., Secrest, J., Du, Z., Zheng, J., Shang, D., Zeng, L., Shao, M., Wang, W., Huang, Y., Wang, Y., Zhu, Y., Li, Y., Hu, J., Pan, B., Cai, L., Cheng, Y., Ji, Y., Zhang, F., Rosenfeld, D., Liss, P. S., Duce, R. A., Kolb, C. E., and Molina, M. J.: Persistent sulfate formation from London Fog to Chinese haze, P. Natl. Acad. Sci. USA, 113, 13630–13635, https://doi.org/10.1073/pnas.1616540113, 2016.

Wang, G., Ma, S., Niu, X., Chen, X., Liu, F., Li, X., Li, L., Shi, G., and Wu, Z.: Barrierless HONO and HOS(O)2-NO_2 Formation via NH_3-Promoted Oxidation of SO_2 by NO_2, J. Phys. Chem. A, 125, 2666–2672, https://doi.org/10.1021/acs.jpca.1c00539, 2021.

Wang, J., Zhang, X., Guo, J., Wang, Z., and Zhang, M.: Observation of nitrous acid (HONO) in Beijing, China: Seasonal variation, nocturnal formation and daytime budget, Sci. Total Environ., 587–588, 350–359, https://doi.org/10.1016/j.scitotenv.2017.02.159, 2017.

Wang, S., Zhou, R., Zhao, H., Wang, Z., Chen, L., and Zhou, B.: Long-term observation of atmospheric nitrous acid (HONO) and its implication to local NO_2 levels in Shanghai, China, Atmos. Environ., 77, 718–724, https://doi.org/10.1016/j.atmosenv.2013.05.071, 2013.

Wang, T., Wei, X. L., Ding, A. J., Poon, C. N., Lam, K. S., Li, Y. S., Chan, L. Y., and Anson, M.: Increasing surface ozone concentrations in the background atmosphere of Southern China, 1994–2007, Atmos. Chem. Phys., 9, 6217–6227, https://doi.org/10.5194/acp-9-6217-2009, 2009.

Wang, T., Xue, L., Brimblecombe, P., Lam, Y. F., Li, L., and Zhang, L.: Ozone pollution in China: A review of concentrations, meteorological influences, chemical precursors, and effects, Sci. Total Environ., 575, 1582–1596, https://doi.org/10.1016/j.scitotenv.2016.10.081, 2017.

Wang, Y., Fu, X., Wu, D., Wang, M., Lu, K., Mu, Y., Liu, Z., Zhang, Y., and Wang, T.: Agricultural Fertilization Aggravates Air Pollution by Stimulating Soil Nitrous Acid Emissions at High Soil Moisture, Environ. Sci. Technol., 55, 14556–14566, https://doi.org/10.1021/acs.est.1c04134, 2021.

Weber, B., Wu, D., Tamm, A., Ruckteschler, N., Rodriguez-Caballero, E., Steinkamp, J., Meusel, H., Elbert, W., Behrendt, T., Sorgel, M., Cheng, Y., Crutzen, P. J., Su, H., and Pöschl, U.: Biological soil crusts accelerate the nitrogen cycle through large NO and HONO emissions in drylands, P. Natl. Acad. Sci. USA, 112, 15384–15389, https://doi.org/10.1073/pnas.1515818112, 2015.

Wong, K. W., Oh, H.-J., Lefer, B. L., Rappenglück, B., and Stutz, J.: Vertical profiles of nitrous acid in the nocturnal urban atmosphere of Houston, TX, Atmos. Chem. Phys., 11, 3595–3609, https://doi.org/10.5194/acp-11-3595-2011, 2011.

Wong, K. W., Tsai, C., Lefer, B., Haman, C., Grossberg, N., Brune, W. H., Ren, X., Luke, W., and Stutz, J.: Daytime HONO vertical gradients during SHARP 2009 in Houston, TX, Atmos. Chem. Phys., 12, 635–652, https://doi.org/10.5194/acp-12-635-2012, 2012.

Wong, K. W., Tsai, C., Lefer, B., Grossberg, N., and Stutz, J.: Modeling of daytime HONO vertical gradients during SHARP 2009, Atmos. Chem. Phys., 13, 3587–3601, https://doi.org/10.5194/acp-13-3587-2013, 2013.

Wu, C., Wu, D., and Yu, J. Z.: Quantifying black carbon light absorption enhancement with a novel statistical approach, Atmos.

Chem. Phys., 18, 289–309, https://doi.org/10.5194/acp-18-289-2018, 2018.

Wu, D., Horn, M. A., Behrendt, T., Müller, S., Li, J., Cole, J. A., Xie, B., Ju, X., Li, G., Ermel, M., Oswald, R., Fröhlich-Nowoisky, J., Hoor, P., Hu, C., Liu, M., Andreae, M. O., Pöschl, U., Cheng, Y., Su, H., Trebs, I., Weber, B., and Sörgel, M.: Soil HONO emissions at high moisture content are driven by microbial nitrate reduction to nitrite: tackling the HONO puzzle, ISME J., 13, 1688–1699, https://doi.org/10.1038/s41396-019-0379-y, 2019.

Wu, Y., Li, S., and Yu, S.: Monitoring urban expansion and its effects on land use and land cover changes in Guangzhou city, China, Environ. Monit. Assess., 188, 54, https://doi.org/10.1007/s10661-015-5069-2, 2015.

Xia, D., Zhang, X., Chen, J., Tong, S., Xie, H.-B., Wang, Z., Xu, T., Ge, M., and Allen, D. T.: Heterogeneous Formation of HONO Catalyzed by CO_2, Environ. Sci. Technol., 55, 12215–12222, https://doi.org/10.1021/acs.est.1c02706, 2021.

Xu, W., Kuang, Y., Zhao, C., Tao, J., Zhao, G., Bian, Y., Yang, W., Yu, Y., Shen, C., Liang, L., Zhang, G., Lin, W., and Xu, X.: NH_3-promoted hydrolysis of NO_2 induces explosive growth in HONO, Atmos. Chem. Phys., 19, 10557–10570, https://doi.org/10.5194/acp-19-10557-2019, 2019.

Xu, Z., Wang, T., Xue, L. K., Louie, P. K. K., Luk, C. W. Y., Gao, J., Wang, S. L., Chai, F. H., and Wang, W. X.: Evaluating the uncertainties of thermal catalytic conversion in measuring atmospheric nitrogen dioxide at four differently polluted sites in China, Atmos. Environ., 76, 221–226, https://doi.org/10.1016/j.atmosenv.2012.09.043, 2013.

Xu, Z., Wang, T., Wu, J., Xue, L., Chan, J., Zha, Q., Zhou, S., Louie, P. K. K., and Luk, C. W. Y.: Nitrous acid (HONO) in a polluted subtropical atmosphere: Seasonal variability, direct vehicle emissions and heterogeneous production at ground surface, Atmos. Environ., 106, 100–109, https://doi.org/10.1016/j.atmosenv.2015.01.061, 2015.

Xue, C., Zhang, C., Ye, C., Liu, P., Catoire, V., Krysztofiak, G., Chen, H., Ren, Y., Zhao, X., Wang, J., Zhang, F., Zhang, C., Zhang, J., An, J., Wang, T., Chen, J., Kleffmann, J., Mellouki, A., and Mu, Y.: HONO Budget and Its Role in Nitrate Formation in the Rural North China Plain, Environ. Sci. Technol., 54, 11048–11057, https://doi.org/10.1021/acs.est.0c01832, 2020.

Xue, L., Gu, R., Wang, T., Wang, X., Saunders, S., Blake, D., Louie, P. K. K., Luk, C. W. Y., Simpson, I., Xu, Z., Wang, Z., Gao, Y., Lee, S., Mellouki, A., and Wang, W.: Oxidative capacity and radical chemistry in the polluted atmosphere of Hong Kong and Pearl River Delta region: analysis of a severe photochemical smog episode, Atmos. Chem. Phys., 16, 9891–9903, https://doi.org/10.5194/acp-16-9891-2016, 2016.

Xue, L. K., Wang, T., Gao, J., Ding, A. J., Zhou, X. H., Blake, D. R., Wang, X. F., Saunders, S. M., Fan, S. J., Zuo, H. C., Zhang, Q. Z., and Wang, W. X.: Ground-level ozone in four Chinese cities: precursors, regional transport and heterogeneous processes, Atmos. Chem. Phys., 14, 13175–13188, https://doi.org/10.5194/acp-14-13175-2014, 2014.

Yabushita, A., Enami, S., Sakamoto, Y., Kawasaki, M., Hoffmann, M. R., and Colussi, A. J.: Anion-Catalyzed Dissolution of NO_2 on Aqueous Microdroplets, J. Phys. Chem. A, 113, 4844–4848, https://doi.org/10.1021/jp900685f, 2009.

Yang, Q.: Observations and sources analysis of gaseous nitrous acid – A case study in Beijing and Pearl River Delta area, PhD thesis, College of Environmental Sciences and Engineering, Peking University, China, 2014.

Yang, Q., Su, H., Li, X., Cheng, Y., Lu, K., Cheng, P., Gu, J., Guo, S., Hu, M., Zeng, L., Zhu, T., and Zhang, Y.: Daytime HONO formation in the suburban area of the megacity Beijing, China, Science China Chemistry, 57, 1032–1042, https://doi.org/10.1007/s11426-013-5044-0, 2014.

Yang, W., Cheng, P., Tian, Z., Zhang, H., Zhang, M., and Wang, B.: Study on HONO pollution characteristics and daytime unknown sources during summer and autumn in Guangzhou, China, China Environmental Science, 37, 2029–2039, https://doi.org/10.3969/j.issn.1000-6923.2017.06.005, 2017.

Yang, W., You, D., Li, C., Han, C., Tang, N., Yang, H., and Xue, X.: Photolysis of Nitroaromatic Compounds under Sunlight: A Possible Daytime Photochemical Source of Nitrous Acid?, Environ. Sci. Tech. Let., 8, 747–752, https://doi.org/10.1021/acs.estlett.1c00614, 2021.

Yang, Y., Shao, M., Keßel, S., Li, Y., Lu, K., Lu, S., Williams, J., Zhang, Y., Zeng, L., Nölscher, A. C., Wu, Y., Wang, X., and Zheng, J.: How the OH reactivity affects the ozone production efficiency: case studies in Beijing and Heshan, China, Atmos. Chem. Phys., 17, 7127–7142, https://doi.org/10.5194/acp-17-7127-2017, 2017.

Yang, Y., Li, X., Zu, K., Lian, C., Chen, S., Dong, H., Feng, M., Liu, H., Liu, J., Lu, K., Lu, S., Ma, X., Song, D., Wang, W., Yang, S., Yang, X., Yu, X., Zhu, Y., Zeng, L., Tan, Q., and Zhang, Y.: Elucidating the effect of HONO on O_3 pollution by a case study in southwest China, Sci. Total Environ., 756, 144127, https://doi.org/10.1016/j.scitotenv.2020.144127, 2021.

Ye, C., Gao, H., Zhang, N., and Zhou, X.: Photolysis of Nitric Acid and Nitrate on Natural and Artificial Surfaces, Environ. Sci. Technol., 50, 3530–3536, https://doi.org/10.1021/acs.est.5b05032, 2016.

Ye, C., Zhang, N., Gao, H., and Zhou, X.: Photolysis of Particulate Nitrate as a Source of HONO and NO_x, Environ. Sci. Technol., 51, 6849–6856, https://doi.org/10.1021/acs.est.7b00387, 2017.

Yu, Y., Galle, B., Panday, A., Hodson, E., Prinn, R., and Wang, S.: Observations of high rates of NO_2-HONO conversion in the nocturnal atmospheric boundary layer in Kathmandu, Nepal, Atmos. Chem. Phys., 9, 6401–6415, https://doi.org/10.5194/acp-9-6401-2009, 2009.

Yue, D. L., Hu, M., Wu, Z. J., Guo, S., Wen, M. T., Nowak, A., Wehner, B., Wiedensohler, A., Takegawa, N., Kondo, Y., Wang, X. S., Li, Y. P., Zeng, L. M., and Zhang, Y. H.: Variation of particle number size distributions and chemical compositions at the urban and downwind regional sites in the Pearl River Delta during summertime pollution episodes, Atmos. Chem. Phys., 10, 9431–9439, https://doi.org/10.5194/acp-10-9431-2010, 2010.

Yue, D. L., Zhong, L., Shen, J., Zhang, T., Zhou, Y., Zeng, L., and Dong, H.: Pollution properties of atmospheric HNO_2 and its effect on OH radical formation in the PRD region in autumn, Environ. Sci. Technol., 39, 162–166, https://d.wanfangdata.com.cn/periodical/hjkxyjs201602030 (last access: 30 June 2022), 2016.

Yun, H., Wang, Z., Zha, Q., Wang, W., Xue, L., Zhang, L., Li, Q., Cui, L., Lee, S., Poon, S. C. N., and Wang, T.: Nitrous acid in a street canyon environment: Sources and contributions to local oxidation capacity, Atmos. Environ., 167, 223–234, https://doi.org/10.1016/j.atmosenv.2017.08.018, 2017.

Yun, H.: Reactive nitrogen ocides (HONO, N_2O_5 and $ClNO_2$) in different atmospheric environment in China: concentrations formation and the impact on atmospheric oxidation capacity, PhD thesis, Department of Civil and Environmental Engineering, The Hong Kong Polytechnic University, China, 2018.

Zha, Q., Xue, L., Wang, T., Xu, Z., Yeung, C., Louie, P. K. K., and Luk, C. W. Y.: Large conversion rates of NO_2 to HNO_2 observed in air masses from the South China Sea: Evidence of strong production at sea surface?, Geophys. Res. Lett., 41, 7710–7715, https://doi.org/10.1002/2014GL061429, 2014.

Zhang, N., Zhou, X., Shepson, P. B., Gao, H., Alaghmand, M., and Stirm, B.: Aircraft measurement of HONO vertical profiles over a forested region, Geophys. Res. Lett., 36, L15820, https://doi.org/10.1029/2009GL038999, 2009.

Zhang, S., Sarwar, G., Xing, J., Chu, B., Xue, C., Sarav, A., Ding, D., Zheng, H., Mu, Y., Duan, F., Ma, T., and He, H.: Improving the representation of HONO chemistry in CMAQ and examining its impact on haze over China, Atmos. Chem. Phys., 21, 15809–15826, https://doi.org/10.5194/acp-21-15809-2021, 2021.

Zhang, W., Tong, S., Ge, M., An, J., Shi, Z., Hou, S., Xia, K., Qu, Y., Zhang, H., Chu, B., Sun, Y., and He, H.: Variations and sources of nitrous acid (HONO) during a severe pollution episode in Beijing in winter 2016, Sci. Total Environ., 648, 253–262, https://doi.org/10.1016/j.scitotenv.2018.08.133, 2019.

Zhao, X., Shi, X., Ma, X., Wang, J., Xu, F., Zhang, Q., Li, Y., Teng, Z., Han, Y., Wang, Q., and Wang, W.: Simulation Verification of Barrierless HONO Formation from the Oxidation Reaction System of NO, Cl, and Water in the Atmosphere, Environ. Sci. Technol., 55, 7850–7857, https://doi.org/10.1021/acs.est.1c01773, 2021.

Zheng, J., Zhong, L., Wang, T., Louie, P. K. K., and Li, Z.: Ground-level ozone in the Pearl River Delta region: Analysis of data from a recently established regional air quality monitoring network, Atmos. Environ., 44, 814–823, https://doi.org/10.1016/j.atmosenv.2009.11.032, 2010.

Zheng, J., Shi, X., Ma, Y., Ren, X., Jabbour, H., Diao, Y., Wang, W., Ge, Y., Zhang, Y., and Zhu, W.: Contribution of nitrous acid to the atmospheric oxidation capacity in an industrial zone in the Yangtze River Delta region of China, Atmos. Chem. Phys., 20, 5457–5475, https://doi.org/10.5194/acp-20-5457-2020, 2020.

Zhong, L., Louie, P. K. K., Zheng, J., Yuan, Z., Yue, D., Ho, J. W. K., and Lau, A. K. H.: Science–policy interplay: Air quality management in the Pearl River Delta region and Hong Kong, Atmos. Environ., 76, 3–10, https://doi.org/10.1016/j.atmosenv.2013.03.012, 2013.

Zhou, X., Civerolo, K., Dai, H., Huang, G., Schwab, J., and Demerjian, K.: Summertime nitrous acid chemistry in the atmospheric boundary layer at a rural site in New York State, J. Geophys. Res.-Atmos., 107, 4590, https://doi.org/10.1029/2001JD001539, 2002a.

Zhou, X., He, Y., Huang, G., Thornberry, T. D., Carroll, M. A., and Bertman, S. B.: Photochemical production of nitrous acid on glass sample manifold surface, Geophys. Res. Lett., 29, 1681, https://doi.org/10.1029/2002GL015080, 2002b.

Zhou, X., Gao, H., He, Y., Huang, G., Bertman, S. B., Civerolo, K., and Schwab, J.: Nitric acid photolysis on surfaces in low-NO_x environments: Significant atmospheric implications, Geophys. Res. Lett., 30, 2217, https://doi.org/10.1029/2003GL018620, 2003.

Zhou, X., Huang, G., Civerolo, K., Roychowdhury, U., and Demerjian, K. L.: Summertime observations of HONO, HCHO, and O_3 at the summit of Whiteface Mountain, New York, J. Geophys. Res.-Atmos., 112, D08311, https://doi.org/10.1029/2006JD007256, 2007.

Zhou, X., Zhang, N., TerAvest, M., Tang, D., Hou, J., Bertman, S., Alaghmand, M., Shepson, P. B., Carroll, M. A., Griffith, S., Dusanter, S., and Stevens, P. S.: Nitric acid photolysis on forest canopy surface as a source for tropospheric nitrous acid, Nat. Geosci., 4, 440–443, https://doi.org/10.1038/ngeo1164, 2011.